The Canadian Mineralogist
Vol. 43, pp. 1711-1734 (2005)

MODIFICATION OF DETRITAL PLATINUM-GROUP MINERALS FROM THE EASTERN BUSHVELD COMPLEX, SOUTH AFRICA

FRANK MELCHER[§], THOMAS OBERTHÜR AND JERZY LODZIAK

Federal Institute for Geosciences and Natural Resources (*BGR*), *Stilleweg 2, D-30655 Hannover, Germany*

ABSTRACT

Platinum-group minerals (PGM) are documented in alluvial sediments in rivers draining the Eastern Bushveld Complex, in South Africa. About 32% of a total of 790 PGM nuggets (50–1600 μm in size) studied show evidence of chemical and textural modifications. Pt–Fe alloys are most susceptible, and reveal a wide spectrum of textural types, among which a Ni- and a Cu-rich assemblage is most common. In the former, Pt–Fe alloy grains [$Pt_{2.3–2.7}Fe$] are concentrically rimmed by layers of ferronickelplatinum [Pt_2NiFe] and coated by an alloy approximating [Ni_2PtFe]. In the Cu-rich assemblage, Pt–Fe alloy [$Pt_{2.2–2.6}Fe$] is concentrically coated by [Pt(Fe,Cu)], *i.e.*, solid solutions of tetraferroplatinum [PtFe] – tulameenite [Pt_2CuFe]. A variety of Pd–Pt–Te–Sb–Sn phases, Au–Ag alloys, and base-metal sulfides are included, and small grains of zvyagintsevite [Pd_3Pb] occur attached to the outer rim. Pt–Fe alloy may also be replaced by heterogeneous Pt–Fe(Cu,Pd) "oxides", which may carry appreciable concentrations of SiO_2 and MgO. Cooperite and braggite, and less commonly sperrylite, are coated by porous native platinum, which also penetrates the grains as root-like channels. Monomineralic grains of porous Pt-rich alloy are considered the end product of this alteration. In rare cases, laurite is replaced by two different types of Ru–Rh–Fe–(Ca–V–Mn) oxides of RuO_2 and RuO stoichiometry; subsequently, the PGE oxide phases are transformed into native ruthenium and rhodium. Palladium-rich oxides are observed in some alteration-induced rims, and are associated with Pd-bearing Fe oxide–hydroxide and Pd-bearing Mn–Fe-rich silicate (*e.g.,* smectite, chlorite). The modified grains are genetically attributed to three processes: (1) sulfidation reactions during magmatic–hydrothermal processes affect Pt–Fe alloy, braggite and Rh sulfides, (2) alteration of Pt–Fe alloy to Pt(Fe,Cu,Ni) alloys at moderate temperature in a reducing environment, and (3) oxidation of PGE sulfides in a low-temperature oxidizing environment. Modification and alteration are suggested to have taken place over an extended period of time, possibly under variable climatic and oxidation conditions during the postmagmatic stage, including serpentinization, during weathering of PGE-bearing bedrock, and after placer deposition.

Keywords: alteration, platinum-group minerals, Bushveld Complex, South Africa.

SOMMAIRE

Les particules de minéraux du groupe du platine (MGP) sont présentes en grand nombre dans les alluvions des rivières drainant la partie orientale du complexe de Bushveld, en Afrique du Sud. Environ 32% d'un total de 790 pépites de MGP, mesurant entre 50 et 1600 μm, font preuve de modifications chimique ou texturale. Les alliages Pt–Fe sont les plus susceptibles, et révèlent une grande variété de types texturaux, parmi lesquels les assemblages à Ni et à Cu sont les plus répandus. Dans le premier groupe, les grains de l'alliage Pt–Fe [$Pt_{2.3–2.7}Fe$] deviennent auréolés par des couches de ferronickelplatinum [Pt_2NiFe] et recouverts d'un alliage de composition voisine de [Ni_2PtFe]. Dans l'assemblage riche en Cu, l'alliage Pt–Fe [$Pt_{2.2–2.6}Fe$] est recouvert de façon concentrique par [Pt(Fe,Cu)], *i.e.*, une solution solide entre tétraferroplatinum [PtFe] et tulameenite [Pt_2CuFe]. Une variété de phases Pd–Pt–Te–Sb–Sn, d'alliages à Au–Ag, et des sulfures de métaux de base sont présents en inclusions, et de petits grains de zvyagintsevite [Pd_3Pb] sont rattachés à la bordure externe. L'alliage Pt–Fe peut aussi se voir remplacer par des "oxydes" hétérogènes de Pt–Fe(Cu,Pd) qui peuvent contenir des concentrations importantes de SiO_2 et MgO. D'autres grains de l'alliage Pt–Fe sont recouverts d'un mince liseré de PtS. Cooperite et braggite, et à un degré moindre, sperrylite, sont recouverts d'une couche de platine natif poreux, qui pénètre les grains aussi en canaux ressemblant un réseau de racines. Des grains monominéraliques d'un alliage poreux riche en Pt représenteraient le terme de ce type d'altération. Dans de rares cas, la laurite est remplacée par deux différents types d'oxydes de Ru–Rh–Fe–(Ca–V–Mn), de stoechiométrie RuO_2 et RuO, respectivement. Par la suite, les oxydes sont transformés en ruthenium et rhodium natifs. Des oxydes riches en Pd sont présents dans la bordure de certains grains ayant subi une altération, et sont associés aux oxydes–hydroxydes palladifères de Fe et aux phases silicatées palladifères riches en Mn et en Fe (*e.g.,* smectite, chlorite). Les grains modifiés sont génétiquement attribuables à trois processus: (1) réactions de sulfuration au cours de processus magmatiques et hydrothermaux affectant l'alliage Pt–Fe, la braggite et les sulfures de Rh, (2) altération de l'alliage Pt–Fe pour donner des alliages Pt(Fe,Cu,Ni) à température moyenne dans un milieu réducteur, et (3) oxydation des sulfures des éléments du groupe du platine dans un milieu oxydant à faible température. Ces modifications et les phénomènes

§ *E-mail address*: f.melcher@bgr.de

d'altération se seraient déroulés sur un grand laps de temps, possiblement sous conditions de climat et d'oxydation variables au cours de stades postmagmatiques, y inclus la serpentinisation, de stades de lessivage des roches du socle porteuses des éléments du groupe du platine, et suite à la déposition des placers.

(Traduit par la Rédaction)

Mots-clés: altération, minéraux du groupe du platine, complexe de Bushveld, Afrique du Sud.

Introduction

Platinum-group minerals (PGM) are found as grains and nuggets ranging in size from 50 μm to (rarely) some centimeters in alluvial and eluvial placers in many locations on Earth (Cabri *et al*. 1996, Weiser 2002). They are commonly regarded as detrital grains, derived from PGM-bearing rocks in the source area by weathering and erosion. A long-lasting discussion, however, has centered on whether all placer grains represent transported particles or whether neoformation may have occurred either in the weathered rock, overlying soils or in placers (*e.g.,* Ottemann & Augusthitis 1967, Cousins 1973, Cousins & Kinloch 1976, Stumpfl 1974, Cabri & Harris 1975, Cabri *et al*. 1996, Bowles 1986, Bowles *et al*. 1994, Weiser 2002). Some of the critical points of this dispute include different sizes of PGM in source rocks (usually small, in the 1–50 μm range) and placers (usually >100 μm), different mineralogical compositions (PGE sulfides, arsenides, antimonides, tellurides, bismuthides in source rocks; Pt–Fe and Ir–Os–(Ru) alloys and sperrylite in placers), different chemical compositions, and different textures.

We have recently documented an impressive assemblage of more than 40 identified species of PGM grains from stream sediments in the vicinity of the original discovery-site (Merensky 1924, 1926, Wagner 1929, Cawthorn 1999) of the Merensky Reef in the Eastern Bushveld Complex (Oberthür *et al*. 2004). The study revealed various features related to alteration of the PGM and triggered the present investigation, in which we describe and develop a classification scheme for altered PGM in the placers of the Eastern Bushveld. In this study, we intend to provide critical new data toward the ongoing dispute on the mobility of platinum-group elements in the exogenic environment.

Samples and Methods

Details about the sampling procedure and mineral separation can be found in Oberthür *et al*. (2004). Selected grains of PGM recovered from 15 sample sites on the farm Maandagshoek were mounted for the preparation of polished sections. A total of 983 quantitative electron-microprobe analyses were performed at 20 kV acceleration voltage and 30 nA sample current (on brass) using a CAMECA SX 100. Counting times were 10 seconds on peak and 5 seconds on each background.

The following X-ray lines, spectrometer crystals and standards (in brackets) were used: S*K*α, PET [(Pt,Pd)S, pyrite], Fe*K*α, LLIF (Fe), Co*K*α, LLIF (Co), Ni*K*α, LLIF (Ni), Cu*K*α, LLIF (Cu), As*L*α, TAP (AsGa), Se*L*α, TAP (Se), Ru*L*α, PET (Ru), Rh*L*α, LPET (Rh), Pd*L*α, LPET (Pd, PdS), Ag*L*β, LPET (Ag), Sn*L*α, PET (Sn), Sb*L*α, PET (Sb), Te*L*α, LPET (Te), Os*M*α, TAP (Os), Ir*L*α, LLIF(Ir), Pt*L*α, LLIF (Pt), Au*L*α, LLIF (Au), Hg*L*α, LLIF (HgS), Pb*M*α, PET (PbS), Bi*M*α, PET (Bi). The Pd*L*β line was used in samples having more than 1% Rh. Background positions were carefully selected to avoid interferences. Peaks of all elements were measured in differential mode to minimize interference problems by overlapping lines of higher than first order. Concentrations of Si, Al, Mg, Na, K, Ca, Mn, V, Cr, and Cl (*K*α lines) were determined in grains containing oxygen, using natural mineral standards. Oxygen (*L*α line on a multilayer crystal) was measured separately at 10 kV, 20 nA using hematite, magnetite and vanadinite standards. Off-line corrections for interference were performed in cases where element concentrations were enhanced by first-order secondary lines by more than 0.1%.

The presence of hydrogen in PGE oxides was tested in a preliminary way using a confocal Raman spectrometer (DILOR LabRAM, Department of Applied Geosciences and Geophysics, University of Leoben) equipped with a frequency-doubled Nd-YAG laser (100 mW, 532.2 nm) and with a He–Ne laser (633 nm), and diffraction gratings of 1200 and 1800 grooves/mm. Detection is with a Peltier-cooled, slow-scan CCD matrix-detector.

Results: PGM Mineralogy

The final concentrates processed from the stream sediments contained 6036 grains of PGM and 406 grains of gold (Gast & Wittich 2001). The largest PGM grain is a Pt–Fe alloy with a maximum diameter of 1.6 mm, and the largest grain of gold is 0.9 mm in diameter (Oberthür *et al*. 2004). A total of 790 PGM-bearing grains derived from five concentrates, including one from a magnetic fraction, were investigated by electron-microprobe techniques. Based on the nature of the main host phase, 64% are Pt–Fe alloys, 17% Pt–

Pd–Ni sulfides, 12% sperrylite, and the remaining are Pd–Sb–As minerals, laurite, Rh sulfides, Pt–(Rh–Ru) alloys and unusual PGM comprising Pd tellurides, Pd sulfide (vasilite), malanite, native platinum and probable PGE oxides and hydroxides (Table 1). Many PGM grains, *e.g.*, 66% of the Pt–Fe grains and 22% of the Pt–Pd–Ni sulfide grains, consist of more than one phase, whereas 93% of the sperrylite grains are monomineralic. Most common are polyphase Pt–Fe alloy grains that are composed of up to seven different PGE phases. These comprise, in order of decreasing abundance, laurite, Ru- or Os-dominated alloys, Rh–(Ir) sulfides (bowieite and miassite), PGE sulfarsenides, Pd–Rh–As phases, Pt–Rh–Ru alloys, PtS, Pd tellurides, unnamed [$Pd_{11}Te_2As_2$], Pt–Rh-bearing thiospinel, Pd–Sb phases, and a number of rare PGM. The composition of the Pt–Fe alloy host phase is Pt-rich (average PGE:BM = 2.6, range 2.2–3.3), in some cases with considerable Pd and Rh (PGE: atom % platinum-group elements, BM: atom % base metals). In Table 2, we extend the findings of Oberthür *et al*. (2004) and summarize all phases identified and their textural setting.

A detailed investigation of the 790 PGM-bearing nuggets revealed that 32% of the nuggets are "altered", *i.e*., they are corroded, replaced or overgrown by secondary phases. From 243 grains classified as being altered, 22% reveal concentric features in the form of one or several rims around a relict core. Fifty-one percent have thin rims, in some cases in addition to concentric features. In 17% of the altered grains, patchy textures were observed, and 41% have a considerable secondary porosity. Complete replacement was observed in 10% of the altered grains. Forty-eight percent of the grains are classified as Pt–Fe alloy hosts, and 23% of the Pt–Pd–Ni sulfides, 4% of the sperrylite, and 8% of the laurite host-grains show alteration features.

Although most of the alteration phases could be identified unequivocally, some phases could not be sufficiently characterized owing to their small grain-size or poor surface-polish (porosity). Some electron-microprobe analyses may pertain to mixtures of various fine-grained phases. The following presentation adheres to an attempt to classify the different alteration-induced assemblages. Alteration or modification phenomena are organized according to the host grain in the order: Pt–Fe alloy, Pt–Pd sulfide, sperrylite, laurite, Rh sulfide (Table 3). Examples of altered grains and specific textures are presented as back-scattered electron images (Figs. 1, 3, 4, 5 and 6) and X-ray element maps (Figs. 2,

TABLE 1. TYPES OF PGM GRAINS INVESTIGATED

	Grain type (host)	Total number	% total	Single %	Composite %	Modified %
1	Pt-Fe alloy	505	64	33	66	48
2	Cooperite, braggite	132	17	78	22	23
3	Sperrylite	94	12	93	7	4
4	Laurite, Rh sulfides, Pt-Rh-Ru alloy, unusual polyphase PGM	19	2	37	63	38
5	Pd-Sb-As minerals	18	2	28	72	33
6	Pt (secondary)	19	2	84	16	100
7	Au-Ag with PGM inclusions*	3	<1	0	100	
Total		790	100	57	43	32

* out of 15 gold grains investigated.

TABLE 2. INVENTORY OF DETRITAL PGM IDENTIFIED IN SAMPLES OF SEDIMENT, FARM MAANDAGSHOEK, EASTERN BUSHVELD COMPLEX*

Platinum-group minerals	Ideal formula	Single grains	Inter-growths	Inclusions	Rims
Pt–Fe alloy	Pt_3Fe – $Pt_{1.5}Fe$	●●●	●●●		○
Tulameenite	Pt_2CuFe	●	●●		●
Ferronickelplatinum	Pt_2NiFe		●●		●
Tetraferroplatinum	Pt(Fe,Ni,Cu)	●	●●		●●
Pt-rich awaruite	Ni_2PtFe		●●		●
Pt–Fe oxides and hydroxides	$(Pt,Fe,Si)_2O$ to PtO_2	●			●
Ru–Rh oxides and hydroxides	RuO_2 to RuO				○
"Palladinite"	PdO				○
Platinum	Pt	●	●		●●
Ru–Os–Ir–Pt alloy		●	●	○	
Pt–Rh alloy		○			
Rhodium	Rh		○		○
Ruthenium	Ru				○
Laurite	RuS_2		●●		
Erlichmanite	OsS_2			○	
Cooperite	PtS	●●	●		○
Braggite	(Pt,Pd)S	●●	○		○
Vysotskite	PdS				○
Bowieite	Rh_2S_3		●		
Miassite	$Rh_{17}S_{15}$		●		
Rh–Fe–Ni sulfide	$(Rh,Fe,Ni)_9S_8$ (?)		●		
Cuprorhodsite – malanite	$CuRh_2S_4$ – $CuPt_2S_4$	○	●		●
Vasilite	$Pd_{16}S_7$	○	●		
Hollingworthite	RhAsS		●		
Irarsite	IrAsS		○		
Sperrylite	$PtAs_2$	●●	○		○
Cherepanovite	(Rh,Ru)As			○	
Rhodarsenide	$(Rh,Pd)_2As$		●		
Palladoarsenide	Pd_2As		●		○
Unnamed	RhNiAs		○		○
Stillwaterite	Pd_8As_3		○		○
Atheneite	$(Pd,Hg)_3As$	○	○		
Stibiopalladinite and mertieite II	$Pd_{5+x}Sb_2$,and $Pd_8(Sb,As)_3$	●	●		●
Isomertieite and mertieite I	$Pd_{11}Sb_2As_2$	●	●		○
Unnamed	$Pd_{11}Te_2As_2$		●		
Unnamed	$(Pd,Rh)_2Sb$			○	
Keithconnite	$Pd_{3-x}Te$		○	○	○
Unnamed	Pd_3Fe		○	○	
Zvyagintsevite	Pd_3Pb		○		●
Atokite–rustenburgite	$(Pd,Pt)_3Sn$			○	
Unnamed	$(Pd,Rh)_3Te_2$			○	
Moncheite	$Pt(Te,Bi)_2$		○	○	
Michenerite	PdBiTe			○	
Sobolevskite	PdBi			○	
Kotulskite	PdTe			○	
Potarite	PdHg	○		○	
Unnamed	Pd(Cu,Te)	○			
Unnamed	Cu_2PdAu		○		

Relative frequency: ●●●: very common, ●●: common, ●: rare, ○: very rare.
* modified from Oberthür *et al.* (2004).

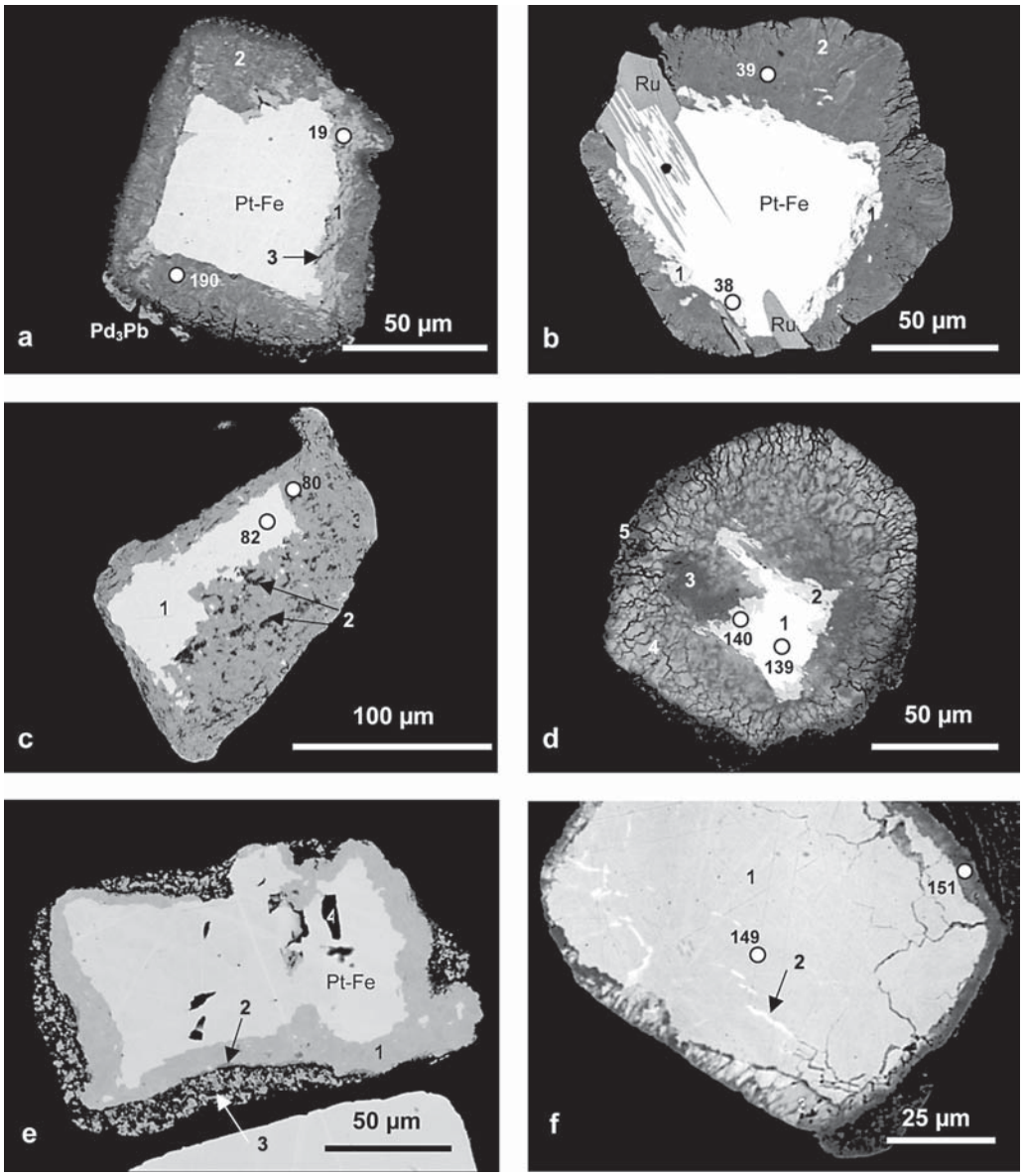

FIG. 1. Nickel-rich alteration of Pt–Fe alloy. Back-scattered-electron images of PGM in polished sections; open circles with numbers refer to analytical results listed in Table 4. a) Grain of Pd-bearing Pt–Fe alloy mantled by ferronickelplatinum (1) and Pt-bearing Ni–Fe alloy (2, probable Pt-bearing awaruite). An unidentified Pd–Cu-rich phase (dark grey, 3) is present in (1). The nugget is partly rimmed by discrete grains of zvyagintsevite [Pd_3Pb]. Sample/grain AS6444/10. b) Grain of Rh–Pd-bearing Pt–Fe alloy intergrown with $Ru_{73}Pt_9Os_6Ir_6Rh_6$ (Ru, grey), surrounded by a thin rim of ferronickelplatinum (1) and a thicker envelope of [Ni_2PtFe] (dark grey, 2). AS6444/21. c) Pt–Fe alloy (1) coated by ferronickelplatinum (3). A Ni-rich phase (2) with PGE/BM = 0.4 is present as patches within the ferronickelplatinum. AS6444/42. d) Altered grain of Pt–Fe alloy (1) rimmed by ferronickelplatinum (2). Pt-bearing Ni–Fe alloy (3) and Ni–Fe–Pt oxide–hydroxide (4) form a thick, inhomogeneous rim. A Pd–Cu–Rh-bearing phase (5) and PGE-free Fe hydroxide (not visible in the image) form the outermost rim of the particle. AS6444/61. e) Grain of Pt–Fe alloy coated by ferronickelplatinum (1). Locally, a thin rind of [Ni_2PtFe] is developed (2), followed by a porous, inhomogeneous rim of [$Pt_{0.8}$(Ni,Fe)] carrying Co, Sb and Bi (3), and by a Mn-bearing chlorite phase (not visible). Pt–Fe alloy has included chalcopyrite (4), sphalerite and millerite (black). AS6465/318. f) Grain of ferronickelplatinum with lamellar structures and irregular areas of a more Pt-rich phase of [$Pt_{1.7}$(Ni,Fe)] composition, overgrown by a thin rim of [Ni_2PtFe] (3). AS6444/64.

4d, 4e). Representative results of chemical analyses of alteration phases displayed in Figures 1–6 are presented in Tables 4 to 7.

Classification and Composition of Altered Pt–Fe Alloy

Oberthür *et al*. (2004) noted that about 68% of the PGM grains consist of single or polyphase grains of Pt–Fe alloy that span a large compositional range from [Pt_3Fe] to [$Pt_{1.5}Fe$]. The distinction of isoferroplatinum [Pt_3Fe] and Pt–Fe alloy (20–50 mol.% Fe) is only possible by X-ray-diffraction analysis (Cabri *et al*. 1996). Therefore, such compositions are referred to as Pt–Fe alloy in the following. Several compositional varieties of Pt–Fe alloy are distinguished, most of which have primary textural attributes (*e.g*., PGE: BM >2.2); these grains commonly carry elevated contents of Rh and Pd. Others, characterized by lower PGE:BM (1.5–2.0) and lack of significant Pd and Rh concentrations, appear to be of secondary origin. Tetraferroplatinum [PtFe], ferronickelplatinum [Pt_2NiFe] and tulameenite [Pt_2CuFe], or solid solutions between these end members, are regarded as secondary minerals on the basis of textural evidence.

About 48% of the Pt–Fe alloy grains are altered. Altered grains carry a variety of [Pt(Fe,Cu,Ni)] phases, a Pt-bearing Ni–Fe alloy phase, PGE oxides

TABLE 3. TEXTURAL CLASSIFICATION OF ALTERATION TYPES

Type	Altered phase	Subtype	Replacement, alteration	Associated minerals	Cases
1	Pt–Fe alloy	1.1	Ni-rich type: $Pt_2NiFe \rightarrow Ni_2PtFe$	Ru alloy, Pd_3Pb	27
		1.2	Cu-rich type		
		1.2.1	Pt(Fe,Cu), concentric	Pd–(Te–Sb–Sn), Au, laurite	69
		1.2.2	$Pt_{1.7-1.8}Fe$ + Pt(Fe,Cu), intergrowth	Pd–Sb, cpy	12
		1.2.3	Pt(Fe,Cu), rare $Pt_{1.5-2.0}Fe$ inclusions	IrAsS, Pd–(Sn–Bi–Te–Pb), cpy, Au	11
		1.2.4	Pt(Fe,Cu) → $Pt_{1.5-2.2}Fe$ rims	Pt alloy	4
		1.3	Porous Pt–Fe alloys and Pt(Fe,Cu)	Pd–Sn–Sb–As–Te, talc	31
		1.4	Pt–Fe oxide/hydroxide	talc	8
		1.5	PtS rims		6
2	Pt–Pd sulfide	2.1	Pt(Pd)	Rh sulfide, Cc, silicates	43
		2.2	PdS		1
3	Sperrylite		(Pt–Fe–Si–O?) → Pt		6
4	Laurite		Ru-rich oxide ⇒ Ru		6
5	Rh sulfide	5.1	$CuRh_2S_4$		11
		5.2	Rh		2

Symbols: Cc: calcite, cpy: chalcopyrite.

TABLE 4. COMPOSITIONS OF Pt–Fe–Ni ALLOYS FOUND IN RIVERS DRAINING THE EASTERN BUSHVELD COMPLEX

Sample	Fig.	Anal.	Mineral	Fe	Co	Ni	Cu	Ru	Rh	Pd	Sb	Os	Ir	Pt	Σ
AS6444	1c	82	Pt–Fe alloy	10.39		0.21	0.22		0.11	1.49			0.74	86.81	99.97
AS6444	1d	139	Pt–Fe alloy	10.36		0.25	0.33	0.14	0.60	0.49			0.48	87.78	100.42
AS6444	2a	15	Pt–Fe alloy	10.35		0.19	0.45			2.42			0.14	87.08	100.64
AS6444	1b	38	Nickelferroplatinum	9.12		15.89	0.55	0.32	2.78	0.77				71.80	101.22
AS6444	1d	140	Nickelferroplatinum	8.68		13.96	1.46	0.12	0.16		0.19		0.39	74.47	99.44
AS6444	1a	19	Nickelferroplatinum	12.09	0.21	9.19	1.76		0.42	5.47				68.81	97.95
AS6444	1f	149	Nickelferroplatinum	8.31		16.29	0.53				0.65	0.15		75.01	100.94
AS6444	1a	190	Pt-rich awaruite	14.48	0.57	21.54	1.74		0.82	1.91				60.61	101.67
AS6444	1b	39	Pt-rich awaruite	7.37	0.21	37.34	0.75	0.33	1.52					54.21	101.74
AS6444	1c	80	Pt-rich awaruite	11.72	0.28	31.91	0.68		0.79	0.15		0.11	0.16	55.88	101.68
AS6444	1f	151	Pt-rich awaruite	7.06	0.16	35.37	0.77				0.37			57.44	101.17
AS6444	2a	17	Pt-rich awaruite	8.83	0.34	36.72	0.68		0.23	0.15			0.26	54.85	102.06
AS6444	1c	82	Pt–Fe alloy	1.13		0.02	0.02		0.01	0.09			0.02	2.71	4
AS6444	1d	139	Pt–Fe alloy	1.13		0.03	0.03	0.01	0.04	0.03			0.02	2.73	4
AS6444	2a	15	Pt–Fe alloy	1.11		0.02	0.04			0.14			0.00	2.68	4
AS6444	1b	38	Nickelferroplatinum	0.77		1.28	0.04	0.02	0.13	0.03				1.74	4
AS6444	1d	140	Nickelferroplatinum	0.77		1.18	0.11	0.01	0.01		0.01		0.01	1.90	4
AS6444	1a	19	Nickelferroplatinum	1.07	0.02	0.77	0.14		0.02	0.25				1.74	4
AS6444	1f	149	Nickelferroplatinum	0.72		1.35	0.04				0.03	0.00		1.86	4
AS6444	1a	190	Pt-rich awaruite	1.04	0.04	1.47	0.11		0.03	0.07				1.24	4
AS6444	1b	39	Pt-rich awaruite	0.49	0.01	2.36	0.04	0.01	0.05					1.03	4
AS6444	1c	80	Pt-rich awaruite	0.79	0.02	2.04	0.04		0.03	0.01		0.00	0.00	1.08	4
AS6444	1f	151	Pt-rich awaruite	0.49	0.01	2.31	0.05				0.01			1.13	4
AS6444	2a	17	Pt-rich awaruite	0.58	0.02	2.30	0.04		0.01	0.01			0.00	1.03	4

S, As, Se, Ag, Sn, Te, Au, Hg, Pb, Bi and open fields: below detection limits. The compositions, derived from electron-microprobe data, are first expressed in weight %, then in atoms per formula unit, with the sum of the atoms shown in the last column.

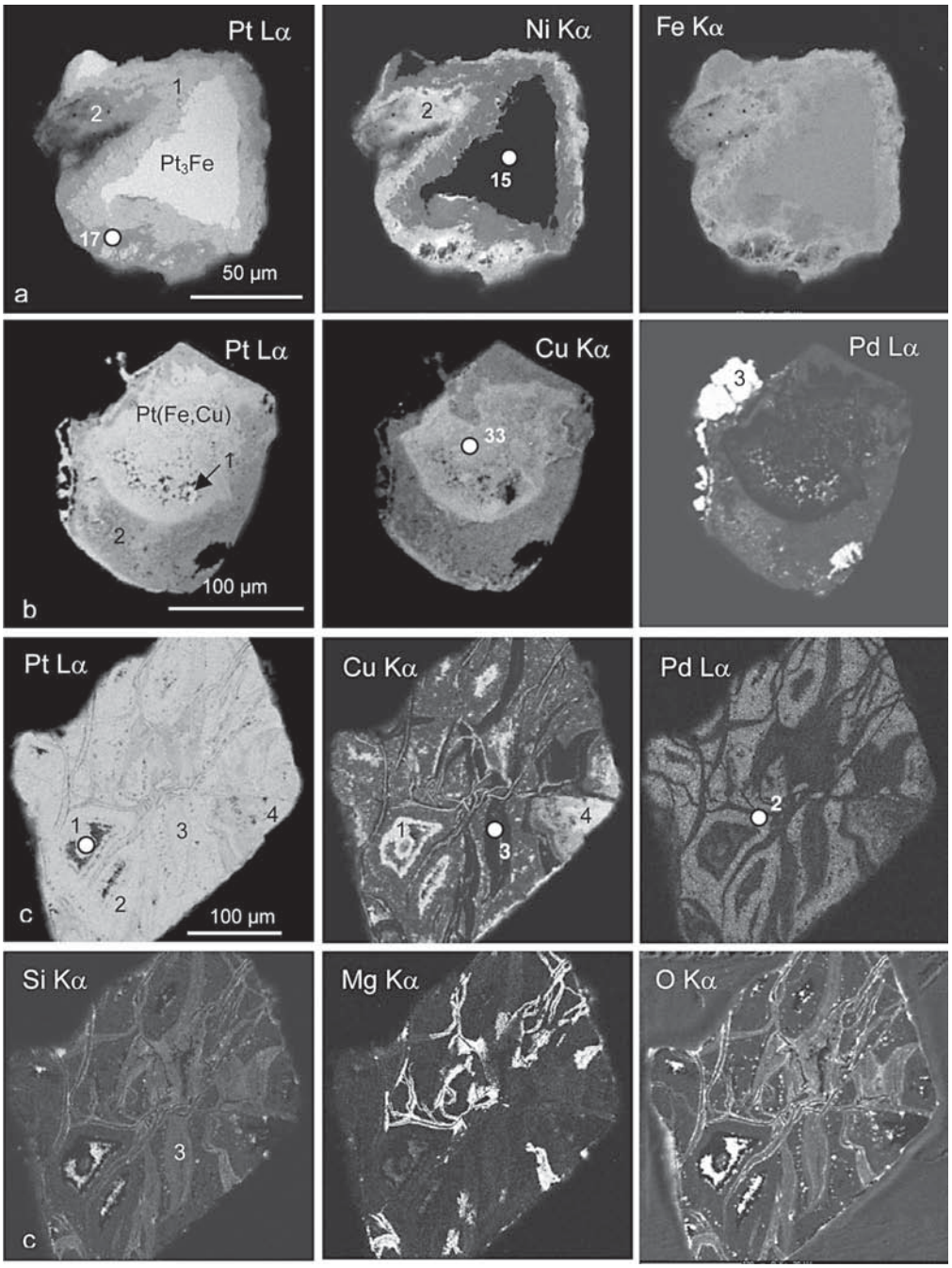

FIG. 2. X-ray element-distribution maps of altered PGM. Open circles with numbers refer to analytical data listed in Tables 4–6. a) Pt–Fe alloy replaced by ferronickelplatinum (1) and Pt-bearing awaruite (2). AS6444/9. b) Altered grain with a core of Pt(Fe,Cu) that has a small inclusion of a Pt-rich alloy phase (1, probable Pt–Fe alloy). The rounded, Cu-rich core is rimmed by an inhomogeneous phase having higher concentrations of Fe and Pd [2]. White spots in core and rim are small discrete grains of zvyagintsevite. The Pd-rich rim is locally overgrown by a thin seam of Cu-rich Pt alloy similar to the core. Large, homogeneous grains of zvyagintsevite (3) occur along the outer margin of the nugget. AS6444/20. c) Altered Pt–Fe alloy grain consisting of a porous mixture of several phases. (1) Pt(Fe,Cu), (2) a Pt–Fe–(Cu–Ni–Pd–SiO_2) phase, (3) flame-like veinlets of a Si–Mg-rich Pt–Fe–(Cu) phase. AS6444/2.

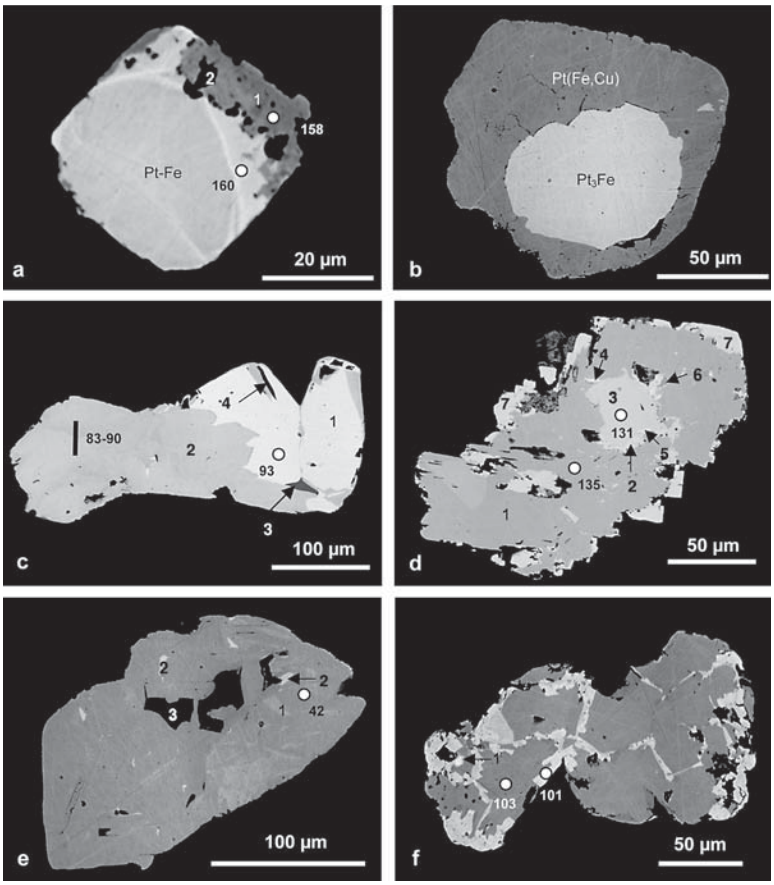

FIG. 3. Alteration of Pt–Fe alloy. Back-scattered electron images of PGM in polished sections; open circles with numbers refer to analytical results listed in Table 5. a) Pt–Fe alloy partly coated by tulameenite (1) with intergrown pentlandite (2). AS6392/101. b) Pt–Fe alloy rimmed by Pt(Fe,Cu). AS6444/23. c) Intergrowth texture of two Pt–Fe alloy phases comprising $Pt_{1.8}Fe$ (1) and Pt(Fe,Cu) (2). A Pd–Sb–(Sn–As–Te) phase (3) and chalcopyrite (4) are included. AS6444/43. d) Pt(Fe,Cu) alloy host (1) with complex inclusion of $Pt_{1.9}Fe$ (2), $Pt_{2.6}Fe$ (3), platinum (4), a Pt–Sn phase (5) and Au–Ag alloy (6). The Pt(Fe,Cu) phase (1) is rimmed by Cu-poor tetraferroplatinum (7) forming a euhedral overgrowth. AS6444/59. e) Inhomogeneous grain of Pt–Fe alloy comprising a matrix of Pt(Fe,Cu) with brighter inclusions of $Pt_{1.3}$(Fe,Cu) (1) and $Pt_{1.8}Fe$ (2). Black inclusions are Al-bearing silicates (3). AS6444/22. f) Tetraferroplatinum (dark grey) intergrown with, and rimmed by Pt–Fe alloy (bright) ranging in composition from $Pt_{1.6}Fe$ to $Pt_{2.2}Fe$. Small spots are Pt-rich alloys (1). AS6444/47.

or hydroxides, and zvyagintsevite [Pd_3Pb]. Textures, combined with chemical compositions, allow distinction of five types: (1) a Ni-rich assemblage, in which Pt–Fe alloy is rimmed by ferronickelplatinum and a Pt-bearing Ni–Fe alloy, (2) a Cu-rich assemblage, in which Pt–Fe alloy is rimmed by tetraferroplatinum–tulameenite solid solutions, (3) porous Pt–Fe alloy, (4) Pt–Fe oxides forming from Pt–Fe alloy, and (5) a rim of PtS on Pt–Fe alloy.

Alteration to Ni-rich alloys

Most of these grains (70–200 µm in size) were recovered from the magnetic fraction, where they are fairly common and conspicuous (type 1.1, Table 3). They invariably have a Pt-rich core (Pt–Fe alloy) and are concentrically surrounded by Ni–Fe-rich Pt alloy (ferronickelplatinum) coated by a Pt-bearing Ni–Fe phase (Fig. 1). Core compositions of Pt–Fe alloy are

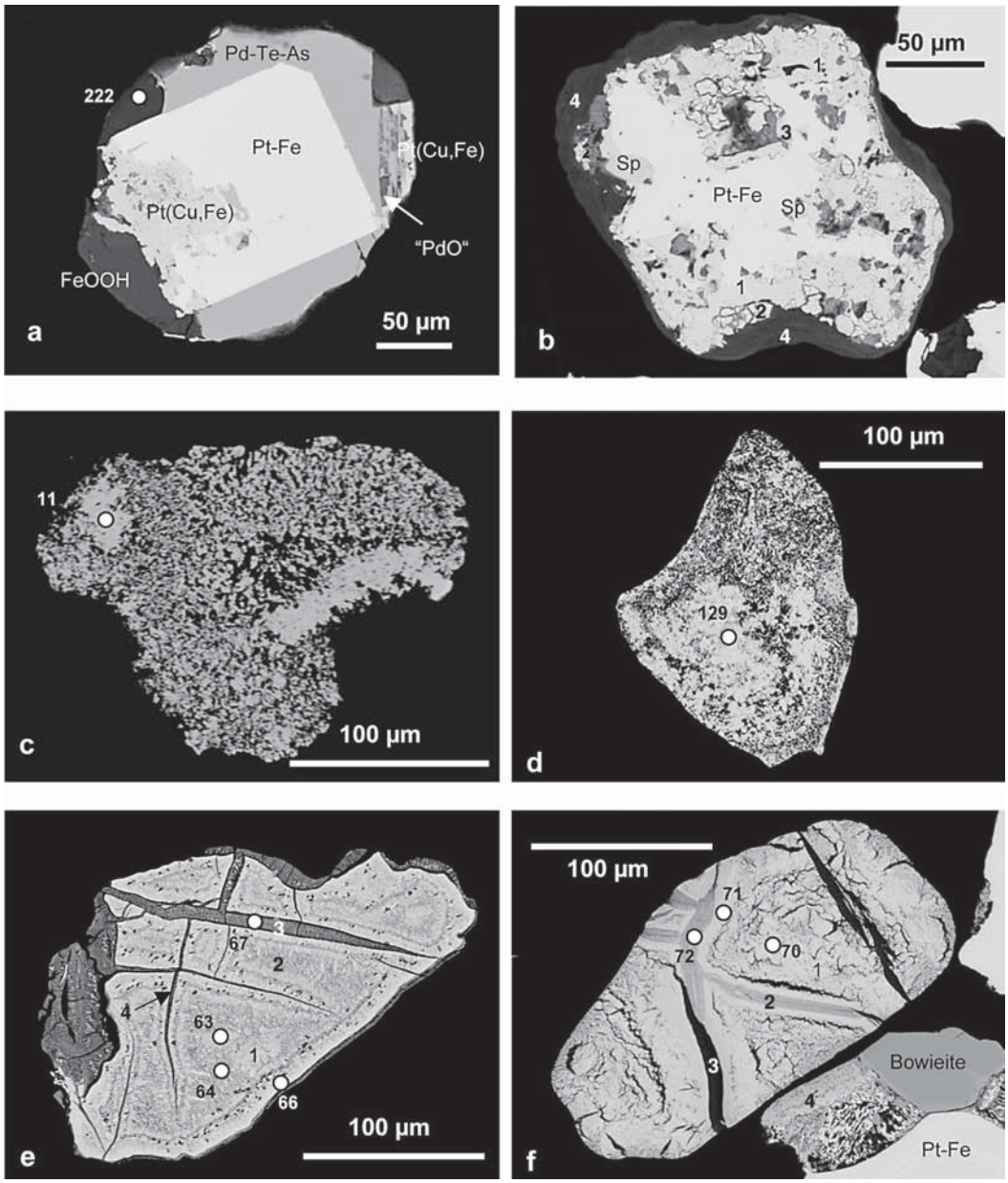

FIG. 4. Alteration of Pt–Fe alloy. Back-scattered electron images of PGM in polished sections; open circles with numbers refer to analytical results listed in Tables 5–7. a) Polyphase grain of Pt–Fe alloy, locally corroded by Pt(Cu,Fe) and overgrown by unnamed [$Pd_{11}Te_2As_2$]; inclusions are keithconnite and kotulskite. The nugget is partly coated by an unusual assemblage consisting of "PdO", Pd-bearing goethite and Pd-bearing silicate (anal. 222, Table 6). AS6392/29, see Figure 5e in Oberthür *et al.* (2004). b) Composite grain of Pt–Fe alloy with sperrylite inclusions (Sp) coated by Pt–Fe oxide (1) and Bi–Sb-bearing Pt oxide (2). Inclusions are Au–Ag and secondary phases carrying Sb, Te and Mn (3). The grain is completely coated by chlorite (4). AS6467/194. c) Porous $Pt_{2.3}Fe$ grain. AS6392/7. d) Porous Pt(Fe,Cu) grain. AS6444/58. e) Altered inhomogeneous Pt–Fe grain with considerable porosity. Patches of more homogeneous Pt(Fe,Cu) (1) are included in a phase of lower PGE/BM and rich in Cu (2). The nugget is veined and rimmed by a Pt–Fe–(Cu–Si–Mg) oxide phase (3). AS6444/31. f) Porous grain of Pt–Fe alloy (1). Veinlets carry talc (3) and a Si–Mg–O-bearing Pt–Fe phase (2). Values of the ratio PGE:BM are similar throughout the grain (1.3–1.4). Polyphase grain in the lower-right corner of the image consists of bowieite with a narrow rim of cuprorhodsite, Pt–Fe alloy, and a porous mixture of Pt–Pd–Fe phases, some of which carry Si and O (4). AS6467/188.

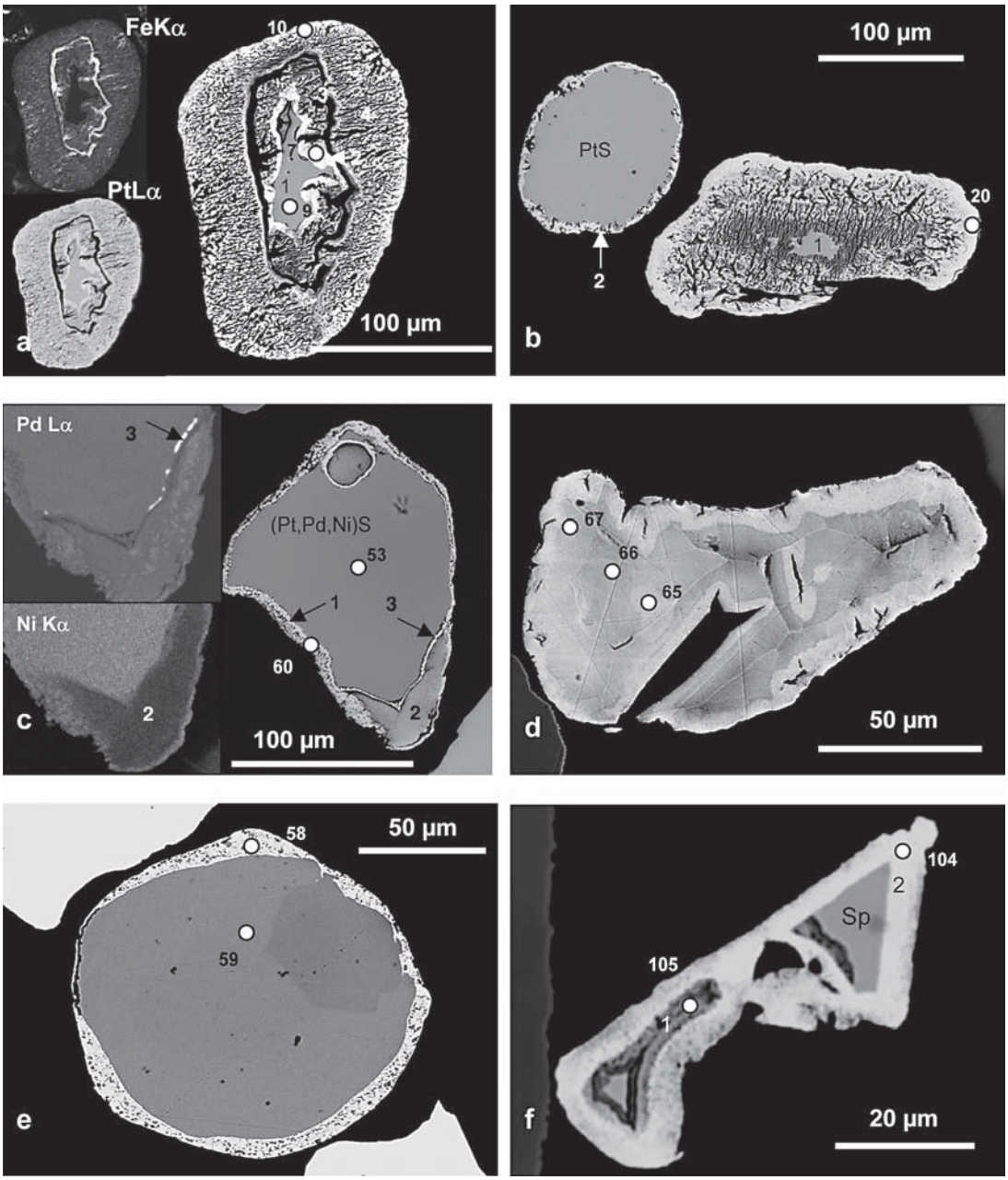

FIG. 5. Back-scattered electron images of PGM in polished sections. Open circles with numbers refer to analytical results listed in Tables 6–7. a) Cooperite (1) replaced by platinum, which occurs as a homogeneous rim (2) or as a porous phase (4). Dark areas (3) are Si–Al–Fe-rich. Insert X-ray maps show the Fe and Pt distributions. AS6435/36. b) Different stages of alteration of cooperite–braggite grains (1) replaced by platinum (2). AS6435/4. c) Braggite coated by a heterogeneous platinum phase which is either rich in Ni and Pd (1), or rich in Pd but low in Ni (2). A narrow zone of an unidentified Pd-rich phase also is present (3). Insert X-ray maps show Pd and Ni distributions. AS6467/121. d) Compositionally homogeneous platinum grain ($10 < Pt/Pd < 12$). AS6467/47. e) Sperrylite rimmed by platinum. AS6465/74. f) Sperrylite (Sp) coated by porous Pt-rich alloy or Pt-(Fe) oxide (1) and pure platinum (2). AS6465/82.

TABLE 5. COMPOSITIONS OF Pt–Fe–Cu ALLOYS FOUND IN RIVERS DRAINING THE EASTERN BUSHVELD COMPLEX

Sample	Fig.	Anal.	Mineral	Fe	Ni	Cu	Rh	Pd	Ag	Sn	Sb	Te	Ir	Pt	Σ
AS6392	3a	160	Pt–Fe alloy	10.73	0.20	0.62	0.10	8.43					0.74	80.50	101.34
AS6444	3c	93	Pt–Fe alloy	12.85	0.22	0.66		0.17						86.14	100.04
AS6444	3d	131	Pt–Fe alloy	12.20	0.45	0.88								86.40	99.92
AS6444	3f	101	Pt–Fe alloy (rim)	10.93	0.23	0.40								88.38	99.94
AS6392	4c	11	Pt–Fe alloy	10.15	0.31	0.93		0.36	0.11					88.80	100.66
AS6444	2b	33	Tulameenite	12.28	0.53	11.79		1.37				0.21	0.13	73.87	100.18
AS6392	3a	158	Tulameenite	12.09	0.29	14.88		10.79						62.72	100.78
AS6444	3d	135	Tulameenite	14.62	1.59	7.09				0.15				76.49	99.93
AS6444	4d	129	Tulameenite	13.16	1.26	10.20		0.95			0.13			74.84	100.54
AS6444	3c	83–90*	Tetraferroplatinum	17.14	0.78	4.27		0.48						77.88	100.55
AS6444	3e	42	Tetraferroplatinum	16.12	1.27	4.19		0.31						77.94	99.82
AS6444	3f	103	Tetraferroplatinum	15.61	1.36	5.63				0.12				77.19	99.92
AS6392	3a	160	Pt–Fe alloy	1.10	0.02	0.06	0.01	0.45					0.02	2.35	4
AS6444	3c	93	Pt–Fe alloy	1.34	0.02	0.06		0.01						2.57	4
AS6444	3d	131	Pt–Fe alloy	1.28	0.04	0.08								2.59	4
AS6444	3f	101	Pt–Fe alloy (rim)	1.19	0.02	0.04								2.75	4
AS6392	4c	11	Pt–Fe alloy	1.10	0.03	0.09		0.02	0.01					2.75	4
AS6444	2b	33	Tulameenite	1.09	0.04	0.92		0.06				0.01	0.00	1.87	4
AS6392	3a	158	Tulameenite	0.99	0.02	1.07		0.46						1.46	4
AS6444	3d	135	Tulameenite	1.32	0.14	0.56				0.01				1.98	4
AS6444	4d	129	Tulameenite	1.16	0.11	0.79		0.04			0.01			1.89	4
AS6444	3c	83–90*	Tetraferroplatinum	1.55	0.07	0.34		0.02						2.02	4
AS6444	3e	42	Tetraferroplatinum	1.48	0.11	0.34		0.01						2.05	4
AS6444	3f	103	Tetraferroplatinum	1.42	0.12	0.45				0.01				2.01	4

S, Co, As, Se, Os, Au, Hg, Pb, Bi and open fields: below detection limits. Compositions, derived from electron-microprobe data, are first expressed in weight %, then in atoms per formula unit, with the sum of the atoms shown in the last column. * Average of a profile with seven spots of similar composition.

characterized by 2.75 < PGE:BM < 2.3 (average 2.4). Occasionally, considerable concentrations of Rh (up to 7.7 at.%) and Pd (up to 10 at.%) are present, along with low Ni (up to 1.5 at.%), and Cu (up to 1.2 at.%) (Figs. 1a–b).

The inner alteration-induced rim is ferronickelplatinum [Pt_2NiFe] with PGE:BM ranging from 0.88 to 1.02 (Figs. 1a–e, 2a, Table 4). The ratio of atomic Ni/(Ni + Cu + Fe + Co) (= X_{Ni}) ranges from 0.45 to 0.62. Maximum concentrations of Rh and Pd are 3.2 and 6.3 at.%, respectively, and Ni concentrations range from 19 to 34 at.%. The outermost rim of the Pt–Fe alloy grains consists of a phase having PGE:BM in the range 0.33–0.54, 0.52 < X_{Ni} < 0.81, and 0.6 < Ni/(Pt + Fe) < 1.7 (Figs. 1a–e, 2a). In that phase, Ni concentrations range from 34 to 61 at.%, Fe from 12 to 25 at.%, and Pt from 23 to 31 at.%. Minor concentrations of Co (up to 1.4 at.%), Cu (up to 4.7 at.%), Rh (up to 3.4 at.%) and Pd (up to 3.3 at.%) are detected. The composition is close to [Ni_2PtFe], suggesting a Pt-bearing analogue of awaruite [Ni_3Fe] with Pt substituting for Ni (*e.g.*, [$(Ni,Pt)_3Fe$]).

Tarkian *et al.* (1996) reported a similar mineral occurring in altered chromitite and suggested that the phase is intermediate between synthetic [$PtFe_3$] and [$PtNi_3$] (Hansen & Anderko 1958, Shunk 1969). PGE-rich awaruite has been described from a number of locations, where it is exclusively associated with chromitite (Ahmed & Bevan 1981, Corrivaux & Laflamme 1990, Kieser 1994).

The chemical variation of Ni-rich alteration is illustrated in triangular diagrams (Figs. 7a, b). In a first step, the Pt–Fe alloy is transformed into almost stoichiometric ferronickelplatinum, and in a second step, to [Ni_2PtFe], gaining Ni and losing Pt (Fig. 7a). In a Ni–Fe–Cu diagram, ferronickelplatinum compositions do not plot on a common trend with tetraferroplatinum and tulameenite (Fig. 7b), suggesting limited solid-solution.

Most of the Ni-rich nuggets are well rounded, but some retain an original euhedral outline. Seven cases were observed in which the Pt–Fe alloy phase is intergrown with an Ru-rich or Ru–Pt–Rh alloy, or with both (Fig. 1b). Zvyagintsevite [Pd_3Pb] (Fig. 1a),

TABLE 6. COMPOSITION OF PGE "OXIDES", SECONDARY ALLOYS, AND SOME OF THEIR HOST MINERALS

Sample	AS 6444	AS 6444	AS 6444	AS 6444	AS 6444	AS 6444	AS 6444	AS 6467	AS 6467	AS 6467	AS 6465	AS 6467	AS 6467	AS 6467	AS 6467	AS 6467	AS 6465	AS 6392
Figure	2c	2c	2c	4c	4c	4c	4c	4d	4d	4d	4f	6a	6a	6a	6a	6a	6c	4a
Anal. No.	1	2	3	63	64	66	67	70	71	72	105	23	25	26	27	177	33	222
Mineral	Tul	Pt–Fe ox	Pt–Fe ox	PtFe	Pt–Fe ox	PtFe	Pt–Fe ox	Pt–Fe	Pt–Fe ox	Pt–Fe ox	Pt ox	Lrt	Ru oxide	Ru oxide	Ru oxide	Ru alloy	Rh alloy	smectite?
O wt.%	0.93	4.12	6.78	3.20	7.83	1.88	10.64		2.29	11.94	8.18		27.34	26.55	14.48	3.33	1.53	26.39*
Mg		0.09	0.14		0.70		1.93		0.17	2.32	0.39		0.29	0.37				2.43
Al		0.61	1.35		0.36		0.96		0.17	0.18	0.46		0.34	0.36	0.18			1.18
Si	0.13	1.39	2.97	0.68	1.60	0.37	3.59	0.26	1.39	5.31	4.42		0.27	0.29	1.16			12.59
S				0.24	0.11	0.17					0.10	37.03	0.17			0.17	0.12	0.24
Cl													0.60	0.62	0.15			0.18
Ca		0.05	0.15				0.12		0.11	0.14	0.19		1.62	1.56	0.69			1.65
Ti															0.31			
V													1.87	2.18	0.33			
Mn													1.65	1.66	1.33	0.29		9.29
Fe	12.55	11.86	10.18	14.87	12.53	13.10	11.97	16.26	15.33	12.61	3.33		0.25	0.22	5.07	2.62	0.28	18.19
Co															0.37	0.61		1.12
Ni	1.10	0.68	0.23	3.19	1.99	1.54	0.99	0.53	0.51	0.26			2.02	1.59	1.68	2.37		1.38
Cu	10.60	1.87	0.53	3.88	5.67	9.38	5.42	0.23	0.90	0.30			0.42	0.56				0.13
As											0.12	0.19						
Se				0.11														
Ru												54.10	56.81	57.78	47.99	63.34	1.94	
Rh												2.30	2.16	1.96	15.64	23.40	89.94	
Pd	0.16	1.99	0.16	0.33		0.19		2.27	2.34	0.80								3.56
Ag			0.11					0.14										
Sb																	0.45	
Os												4.94			7.64	4.21		
Ir												0.47	1.03	1.09	1.22	0.62	0.44	
Pt	75.36	77.41	78.55	71.83	70.04	71.64	63.78	79.88	78.90	62.19	80.85	0.16		0.31	0.40	0.50	3.58	0.60
Pb													0.56	0.58				
Bi				0.17			0.14											
Total	100.84	100.07	101.17	98.49	100.82	98.26	99.54	99.57	102.12	96.05	98.05	99.19	97.41	97.66	98.63	101.46	98.28	79.46§
O at.%	6.76	25.64	35.64	20.27	37.69	12.86	42.78		15.34	46.59	43.12		68.10	67.24	49.95	17.37	9.39	57.16*
Mg		0.35	0.48		2.20		5.09		0.76	5.95	1.36		0.47	0.62				3.47
Al		2.27	4.22		1.04		2.30		0.69	0.41	1.45		0.51	0.54	0.37			1.51
Si	0.54	4.92	8.90	2.44	4.38	1.44	8.22	1.26	5.31	11.80	13.28		0.38	0.41	2.28			15.53
S				0.76	0.26	0.59					0.26	66.22	0.22			0.44	0.38	0.26
Cl													0.67	0.71	0.23			0.17
Ca		0.13	0.32				0.19		0.29	0.21	0.40		1.61	1.58	0.95			1.43
Ti															0.36			
V													1.47	1.73	0.35			0.03
Mn													1.20	1.23	1.33	0.45	0.00	5.86
Fe	26.10	21.18	15.34	26.98	17.28	25.68	13.78	39.06	29.43	14.09	5.03		0.18	0.16	5.01	3.91	0.50	11.29
Co															0.34	0.85		0.66
Ni	2.18	1.16	0.33	5.50	2.61	2.87	1.08	1.20	0.93	0.28			1.37	1.10	1.58	3.37		0.82
Cu	19.37	2.94	0.71	6.19	6.88	16.16	5.48	0.48	1.52	0.30			0.26	0.36				0.07
As											0.14	0.14						
Se				0.15														
Ru												30.68	22.40	23.16	26.20	52.30	1.89	
Rh												1.28	0.84	0.77	8.39	18.98	85.80	
Pd	0.18	1.86	0.13	0.32		0.20		2.87	2.36	0.47								1.16
Ag			0.08					0.18										
Sb																	0.04	
Os												1.49			2.22	1.85		
Ir												0.14	0.21	0.23	0.35	0.27	0.22	
Pt	44.87	39.55	33.86	37.32	27.66	40.21	21.03	54.94	43.36	19.90	34.95	0.05		0.06	0.11	0.21	1.80	0.11
Pb													0.11	0.11				
Bi				0.08			0.04											
Total	100	100	100	100	100	100	100	100	100	100	100	100	100	100	100	100	100	100

Na, K, Cr, Sn, Au, Hg and open fields: below detection limits. Compositions, derived from electron-microprobe data, are first expressed in weight %, then in atom %. * Oxygen established by stoichiometry; § The total includes 0.23% Na and 0.11% K. Symbols: Lrt: laurite, Tul: tulameenite.

a Pt–Ni–Fe oxide phase, a Ru(Rh,Fe) oxide phase, an unidentified Rh–Sb–Cu mineral (Figs. 1a, d), chlorite, Fe oxide–hydroxide (Figs. 1d–e), and calcite also were found in the outermost rim. In one case, sphalerite, a Ni sulfide, and chalcopyrite are present as inclusions in the Pt–Fe alloy (Fig. 1e). Internal textures in the alteration rims include tubes, channels, channel networks (Figs. 1a, b, d, 2a) and occasionally spotted patterns with small areas of Ni-rich alloy heterogeneously distributed within ferronickelplatinum (Fig. 1c). X-ray maps show that Pd is commonly enriched along the outer rims of nuggets, forming discrete tiny grains of phases such as zvyagintsevite [Pd_3Pb].

A few grains were discovered where the above described concentric pattern is modified. These are composed of ferronickelplatinum having lamellar structures and more irregular areas of a Pt-rich phase approximating [$Pt_{1.7}$(Ni,Fe)] in composition (Fig. 1f), and a thin, inhomogeneous rim of [$(Ni,Fe)_{2.5}Pt$].

Alteration to Cu–Fe-rich alloy

Pt–Fe alloy is commonly associated with a solid solution of tetraferroplatinum [PtFe] and tulameenite [Pt_2CuFe], which are structurally closely related and show extensive miscibility (Bowles 1990). For simplicity, they are referred to as [Pt(Fe,Cu)] throughout the paper (type 1.2, Table 3, Figs. 7b, c). Three types of association are recognized: (1) rims of [Pt(Fe,Cu)] on Pt–Fe alloy, (2) oriented intergrowths of [Pt(Fe,Cu)] on Pt–Fe alloy, and (3) other types.

A concentric or partial rim around Pt–Fe alloy grains is most frequent; these nuggets are well rounded (type 1.2.1, Figs. 3a, b, 4a, b). The Pt–Fe alloy varies in composition from $Pt_{1.7}Fe$ to $Pt_{2.6}Fe$, with most grains being in the range $Pt_{2.3–2.5}Fe$. Palladium concentrations are usually low (<2 at.%), but may reach values as high as 20 at.%. The [Pt(Fe,Cu)] rim varies from [$Pt_{0.92}$(Fe,Cu)] to [$Pt_{1.14}$(Fe,Cu)] in composition, and X_{Cu} = Cu/(Cu + Ni + Fe + Co)] ranges from 0.04 to 0.50. Palladium concentrations are lower than in the Pt–Fe alloy grains, with occasional enrichment only (up to 5.7 at.% Pd). Some of the concentrically altered grains have inclusions of kotulskite [PdTe] and sperrylite [$PtAs_2$] in the host Pt–Fe alloy (Fig. 4a). More common are inclusions of keithconnite, stibiopalladinite, rustenburgite, Au–Ag alloy, laurite and pentlandite (Fig. 3a) in the [Pt(Fe,Cu)] rim phase. Hollingworthite, unnamed [$Pd_{11}Te_2As_2$], keithconnite, palladoarsenide, Ru-dominant alloy, and complex hydroxide minerals are found attached to the alteration rim.

TABLE 7. COMPOSITIONS OF Pt–Pd SULFIDES, SPERRYLITE AND Pt–Pd ALLOYS FOUND IN RIVERS DRAINING THE EASTERN BUSHVELD COMPLEX

Sample	Fig.	Anal.	Mineral	S	Fe	Ni	As	Se	Pd	Ag	Sb	Ir	Pt	Σ
AS6435	5a	9	Cooperite	14.76		0.58			1.43				82.68	99.45
AS6467	5c	53	Braggite	16.89		2.20			19.52				61.04	99.66
AS6465	5e	59	Sperrylite	0.12			41.26	0.13			0.97	0.11	56.54	99.12
AS6435	5a	7	Platinum	0.12	0.55				1.45	0.14			97.43	99.69
AS6435	5a	10	Platinum		0.17	0.10			4.55		0.11		95.33	100.27
AS6435	5b	20	Platinum	0.11		0.28			1.15				99.08	100.63
AS6467	5c	60	Platinum			1.83			15.24	0.11			82.45	99.63
AS6467	5d	65–67*	Platinum	0.29		0.11			4.56				94.23	99.19
AS6465	5e	58	Platinum		0.12		0.19				0.97	0.31	99.67	101.27
AS6465	5f	104	Platinum		1.04						0.20		99.41	100.65
AS6435	5a	9	Cooperite	50.73		1.08			1.48				46.70	100
AS6467	5c	53	Braggite	49.68		3.53			17.29				29.50	100
AS6465	5e	59	Sperrylite	0.43			64.47	0.19			0.93	0.07	33.92	100
AS6435	5a	7	Platinum	0.70	1.88				2.59	0.25			94.60	100
AS6435	5a	10	Platinum		0.56	0.32			7.97		0.17		90.98	100
AS6435	5b	20	Platinum	0.67		0.92			2.05				96.37	100
AS6467	5c	60	Platinum			5.20			23.96	0.17			70.67	100
AS6467	5d	65–67*	Platinum	1.67		0.34			7.99				90.00	100
AS6465	5e	58	Platinum		0.42		0.49				1.52	0.31	97.26	100
AS6465	5f	104	Platinum		3.53						0.31		96.17	100

Co, Cu, Ru, Rh, Sn, Te, Os, Au, Hg, Pb, Bi and open fields: below detection limits. Compositions, derived from electron-microprobe data, are first expressed in weight %, then in atom %. * Average of three similar measurements.

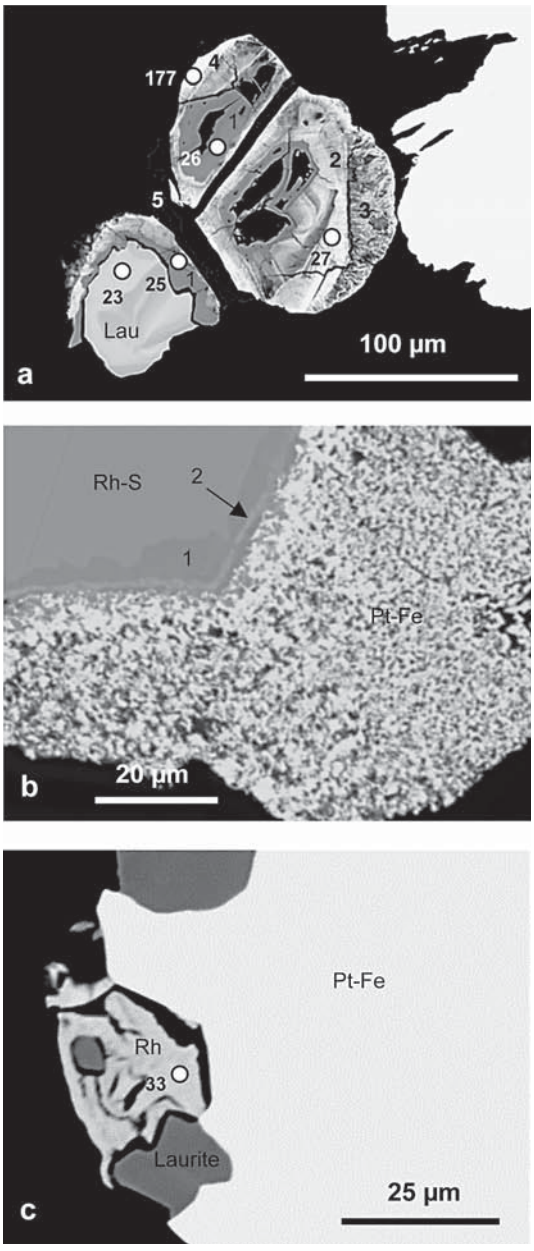

FIG. 6. Back-scattered electron images of PGM in polished sections. Open circles with numbers refer to analytical results listed in Tables 6 and 7. a) Laurite (Lau) decomposed to a variety of Ru–Rh-rich oxides–hydroxides (1–3) and Ru alloy (4). Fe oxide (5) between grains barely visible. AS6467/154. b) Bowieite (Rh–S) with narrow rim of cuprorhodsite (1) and Pt-rich cuprorhodsite (2, bright) at contact with porous Pt–Fe alloy. AS6467/168. c) Rhodium with dehydration textures at margin of Pt–Fe alloy (Pt–Fe) and laurite. AS6465/160.

Pt–Fe alloy and [Pt(Fe,Cu)] may form regular, oriented intergrowth textures in euhedral or anhedral grains; in addition, they have inclusions of stibiopalladinite and related phases, as well as chalcopyrite, cubanite and pyrrhotite (type 1.2.2, Figs. 3c, d). The composition of the Pt–Fe alloy differs from the above group by lower

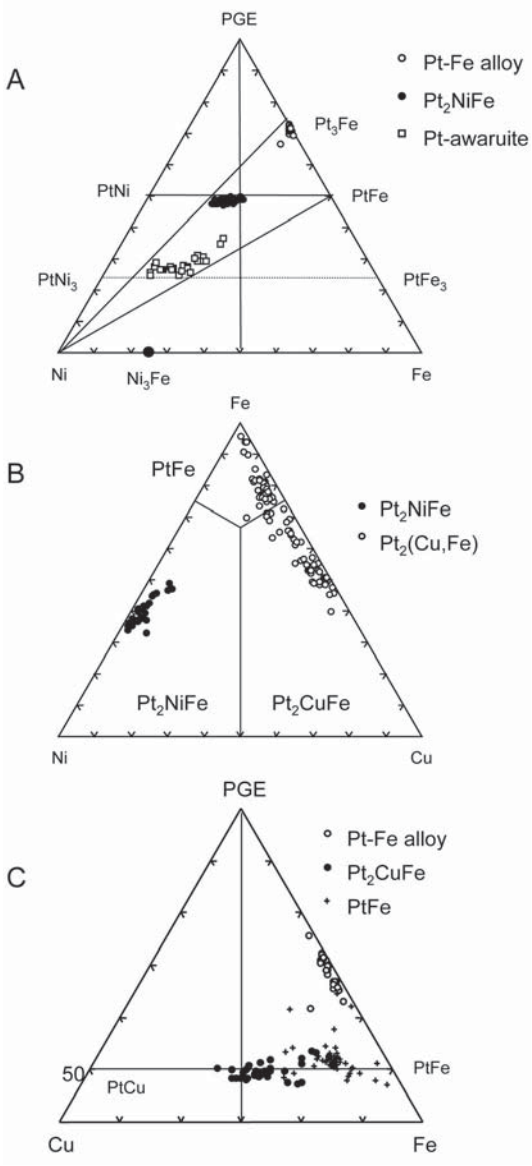

FIG. 7. Triangular diagrams illustrating the composition of phases in terms of PGE–Ni–Fe and PGE–Cu–Fe. a) The Ni-rich assemblage of alteration phases. b) The Pt(Fe,Cu,Ni) minerals. c) The host and rim phases of the Cu-rich type of alteration assemblage.

concentrations of Pt ([$Pt_{1.7–1.8}Fe$]) at low Pd and Cu. The [Pt(Fe,Cu)] phase is also poor in Pd and has moderate Cu concentrations (X_{Cu} in the range 0.14–0.27). Element mapping (not shown) of the grain displayed in Figure 3c reveals abundant elongate Pd-rich inclusions in the bright $Pt_{1.8}Fe$ phase.

Other grains either lack a Pt–Fe alloy phase or have small irregular, patchy inclusions of Pt–Fe alloy only (Pt:Fe = 1.8; type 1.2.3, Fig. 3e). They are tetraferroplatinum with considerable concentrations of Cu (9–18 at.%, X_{Cu} in the range 0.21–0.55), but low Ni and Pd. The grains are neither porous nor coated, but have inclusions of pyrrhotite, chalcopyrite, stibiopalladinite, atokite, irarsite, michenerite, moncheite or Au–Ag–Cu alloy.

An exceptional grain (Fig. 2b) is composed of a [Pt(Fe,Cu)] core with small relics of Pt–Fe alloy, and rimmed by a more Pd-rich alloy. The nugget is spotted with, and overgrown by, anhedral to euhedral grains of zvyagintsevite.

In some cases, homogeneous grains of [Pt(Fe,Cu,Ni)] are rimmed by a thin coating of a Pt-rich alloy [$Pt_{1.5–2.3}$Fe] (type 1.2.4, Table 3, Fig. 3f). The relative proportion of Cu [X_{Cu} = Cu/(Cu + Ni + Fe + Co)] decreases from 0.13 to 0.10 toward these rims. A Pt-rich alloy (Pt:BM = 6.5) is locally present (Fig. 3f).

Porous Pt–Fe alloy

Many individual Pt–Fe-dominant grains are porous (type 1.3, Table 3). In some cases, homogeneous grains are intergrown with, or rimmed by, porous grains. The pores and channel-like structures may contain calcite, Mn carbonate, halite, and various silicates. About 50% of the porous grains are Pt–Fe alloys ([$Pt_{2.2–2.7}Fe$]) carrying low Pd (<1.7 at.%), Cu (<2.2 at.%) and Ni (<0.8 at.%) (Fig. 4c). The remaining domains are tetraferroplatinum and tulameenite (Fig. 4d) that occasionally carry inclusions of atokite or stibiopalladinite.

Mixtures of Pt-rich oxide, hydroxide and silicate

Eight grains were found completely replaced by Pt-rich phases having analytical totals (without oxygen and hydrogen) considerably lower than 100 wt.% (type 1.4, Tables 3, 6; Figs. 2c, 4e, f). The textures of these grains are fairly similar, consisting of porous portions of a more Pt-rich phase (70–80 wt.% Pt) intergrown with flame-like veinlets and rims of a less Pt-rich (65–70 wt.% Pt), but Si- (10–14 wt.% SiO_2) and Mg-bearing (3.5–4.5 wt.% MgO) phase. A talc-like mineral without PGE fills late fractures (phase 3, Fig. 4f).

Compositions of relict oxygen-free phases are close to [Pt(Fe,Cu)] (phase 1 in Figs. 4e, f). In the case of analytical totals lower than 100 wt.%, PGE:BM ratios range from 0.92 to 2.43. The PGE:BM ratio of the original grains may thus be grossly preserved (tetraferroplatinum and Pt–Fe alloy). However, intermediate values from 1.3 to 1.5 also are common. Iron dominates among the base metals (X_{Fe} in the range 0.57–0.96), but Cu (up to 18 at.%) and Ni (up to 7 at.%) are commonly present. Some grains have up to 22 at.% Pd, but all other PGE are below the detection limit of the electron microprobe. Raman analyses using a Nd–YAG laser (532.2 nm) failed to detect OH groups or H_2O in the oxygen-bearing phases. The spectra are devoid of any bands, and are similar to the infrared-absorption spectra of an unnamed Pd–Pb oxide from Penikat (Barkov *et al.* 1999).

The Pt–Fe "oxides" analyzed are a rather heterogeneous group composed mainly of Pt (10–70 at.%), Fe (5–35 at.%) and O (1–60 at.%). The concentrations of Si (up to 9 at.%) and Mg (up to 6 at.%) correlate well with oxygen. Metal:oxygen ratios range from 0.5 to 7, with a maximum between 1 and 3 (Fig. 8a), representing variable compositions between ideal "PtO_2", "Pt_3O_4" and "PtO", and extending to even more metal-rich compositions. The PGE:BM ratios cluster close to 1, 1.5 and 2–2.4. In diagrams of PGE–BM–O and PGE–BM–Si(+ Al + Mg + Ca), the Pt-bearing oxides follow trends at constant PGE:BM ratios from low to high oxygen and silica concentrations, respectively (Figs. 8a, b). In Pt–Fe oxides reported from the ferromagnetic fraction of alluvial mineralization and *in situ* chromitite in New Caledonia (Augé & Legendre 1994), atomic metal:oxygen ratios range from 9 to 1. Their PGE:BM values are similar to those described in the present study (Fig. 8a), but Augé & Legendre (1994) did not report concentrations of non-metallic elements except oxygen.

Rims of PtS on Pt–Fe alloy

Very thin seams of PtS (probably cooperite) mantling Pt–Fe alloy have been observed (type 1.5, Table 3) in rare cases. Occasionally, the PtS phase is found also to replace the Pt–Fe alloy host. Such grains may be associated with chromian magnetite and silicates.

Classification and Composition of Altered Pt–Pd–Ni Sulfides

Rims of native platinum

Grains of Pt–Pd–Ni sulfides (cooperite, braggite) show characteristic concentric patterns of alteration (type 2.1, Table 3, Figs. 5a–c). Most (78%) of the Pt–Pd–Ni sulfide grains are monophase and intergrown with bowieite, miassite and laurite (Oberthür *et al.* 2004). Two compositional varieties of Pt–Pd–Ni sulfides are observed in an altered state. One (presumably cooperite) carries 0.6–1.5 at.% Ni and 0.7–5.4 at.% Pd, the other (presumably braggite) has up to 3.5 at.% Ni and up to 17.3 at.% Pd. The relative proportion of altered cooperite grains seems to be larger than

altered braggite grains (85% of the altered grains are close to PtS in composition).

Most commonly, relics of primary Pt–Pd–Ni sulfides are rimmed by a porous Pt-rich alloy phase (native platinum) with abundant root-like channels that occasionally form a dense network penetrating into the Pt–Pd sulfide (Figs. 5a, b). In some cases, a more homogeneous outer rim of nearly the same composition follows. X-ray maps reveal that the channels carry elevated contents of Fe and Si, but less Pt, Ni and Pd, than the Pt-rich zones (Fig. 5a). The platinum rims have low concentrations of most minor elements, except for Ni (up to 5.2 at.%) and Pd (up to 30 at.%); platinum concentrations range from 64 to 97 at.%. In most grains, Ni concentrations decrease and Pt/Pd values increase from sulfide cores to the platinum rims; however, areas of higher contents of Pd and Ni in rims also are present (Fig. 5c). Enrichment of Pd in the rims is confined to either very narrow zones (a few μm thick) or to distinct spots. Distinctly elevated Ni contents were observed in narrow rims of a zoned "braggite" grain (Fig. 5c), as were Fe-rich zones in rare cases, either rimming relict sulfide domains (Fig. 5a) or filling channels.

Seventeen grains of native platinum without relict phases have been found. They are porous, and may be rimmed by a more homogeneous phase of similar composition. Concentrations of Fe (up to 1.1 at.%), Cu (up to 0.1 at.%), Ni (up to 2.2 at.%) and S (up to 2.8 at.%) are low; those of Pd may reach 10 at.%, and the Pt:Pd ratio ranges from 10 to 50. Occasional zoning in BSE images results from different porosities rather than compositions (Fig. 5d). The textures suggest that the porous grains of native platinum are end-products of Pt–Pd–Ni sulfide alteration. Thus, most of the native platinum grains detected in the SEM study of Oberthür *et al*. (2004) originated from the alteration of Pt–Pd–Ni sulfides.

PdS on (Pt,Pd,Ni) sulfide

In one case only, braggite (28 at.% Pt, 21% Pd and 2.5% Ni) was partly mantled by a very thin rim of "PdS" (47 at.% Pd, 3% Pt, 5% Ni; vysotskite) (type 2.2, Table 3). However, in a number of cases, Pd enrichment was noted in Pt–Pd–Ni sulfide along rims and cracks.

Composition of Altered Sperrylite

Sperrylite is usually unaltered. However, a few grains have narrow (<10 μm thick, Fig. 5e), partly discontinuous rims of pure platinum (>96 at.%) with minor impurities of Fe (<0.4 at.%), As (0.5–0.7 at.%), Ru (<0.3 at.%), Sb (0.5–2.1 at.%) and Ir (<0.3 at.%). The sperrylite host crystals carry Se (0.2–0.3 at.%), S (0.6–2.5 at.%) and Sb (0.1–0.9 at.%) besides major Pt and As. X-ray maps show that Fe-rich phases having low concentrations of Pt may be included in the alteration rim. Only one grain (Fig. 5f) was found with almost complete alteration of sperrylite involving a first, probable Pt–Fe oxide transition stage, followed by an outer rim of pure platinum.

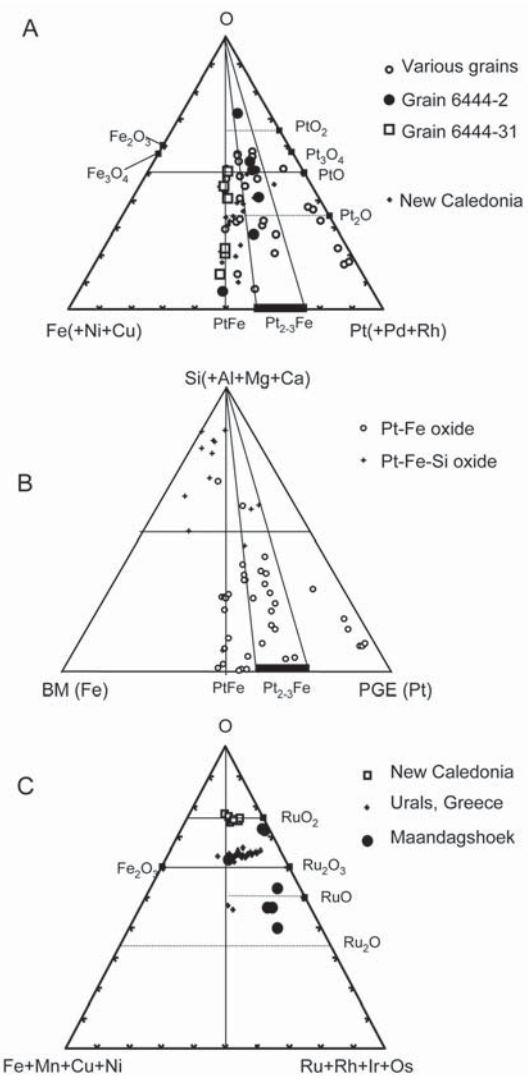

FIG. 8. Triangular diagrams illustrating compositions of PGE oxides. a) PGE–BM–O diagram showing the Pt–Fe oxides from Maandagshoek; the variation in two grains is illustrated separately (Figs. 2c, 4e). Pt–Fe oxide phases from New Caledonia (Augé & Legendre 1994) are shown for comparison. b) PGE–BM–Si diagram for Pt–Fe oxides from Maandagshoek. c) PGE–BM–O diagram for Ru-rich oxides–hydroxides. Analytical data from Augé & Legendre (1994: New Caledonia) and from Garuti *et al*. (1997: Urals) and Garuti & Zaccarini (1997: Greece) are added for comparison.

Alteration Phenomena in Laurite: Ru Oxide or Hydroxide and Ru-Rich Alloy

Laurite [RuS_2] is commonly intergrown with Pt–Fe grains. Crystals are usually euhedral and compositionally zoned with respect to Os (Oberthür *et al.* 2004). The alteration of laurite is, however, uncommon (type 4, Table 3). In two examples only, inhomogeneous oxygen-bearing Ru-rich phases have been found. Ru-rich oxides replacing laurite (Fig. 6a) show more homogeneous patchy areas (phase 1 in Fig. 6a) that are composed of 54–58 wt.% Ru, 27% O, 1–3% Rh, V, Ni, Mn and Ca, and <1% Si, Al, Fe, Mg, Cu and Cl; totals are 95–97 wt.% only, suggesting the additional presence of hydrogen (Table 6). The metal:oxygen ratio points to a composition close to RuO_2 (Fig. 8c). The homogeneous area is replaced or coated by an inhomogeneous mixture having lower Ru (36–50 wt.%) and O (6–14 wt.%), but higher Rh (6–16 wt.%) and Fe (5–11 wt.%), and some Os, Ni, Mn, V, Co, Ti, Ca and Si (phase 2 in Fig. 6a, Table 6). The metal:oxygen ratio is intermediate between Ru_2O and RuO. Poor analytical totals of some domains also suggest the presence of hydrogen. Raman spectroscopy (Nd–YAG laser, 532.2 nm), however, failed to prove the presence of OH groups or H_2O. In contrast to the host laurite, which gives a characteristic Raman spectrum, the spectra of the Ru oxides are virtually without any significant bands. In phase 3 (Fig. 6a), some of the PGE are not bound to oxygen, probably owing to formation of fine-grained alloy phases. A Ru–Rh alloy phase in places rims the oxides (phase 4, Fig. 6a). Magnetite and Fe-hydroxide lacking significant PGE (about 0.1 wt.% Ru) are present as cementing phases between two altered grains of laurite (phase 5, Fig. 6a).

The second Ru-rich oxide grain is attached to Pt–Fe alloy coated by ferronickelplatinum and Pt-bearing Ni–Fe alloy. No primary Ru phase is preserved. The oxide phase is inhomogeneous and carries 37–60 wt.% Ru, 8–15% Rh, 6–25% Fe, 2–11% Os, 2% Si and 9–12% O; [4 < Ru/Rh < 5; 3 < PGE:BM < 5. The metal-to-oxygen ratio ranges from 1.3 to 1.8 (Fig. 8c). The Ru oxide is intergrown with Ir-bearing goethite (3.6–5.0 wt.% Ir, 0.8–1.2% Rh, 0.2–0.4% Ru, 0.2–2.3% Pt). Some laurite grains and aggregates of laurite and Rh sulfide are coated by a porous Ru-rich alloy. Its composition ranges from $Ru_{62}Rh_{23}Os_2Fe_5Ni_4$ to $Ru_{86}Rh_4Fe_5$, and is thus different from those Ru–Rh–Pt–Fe alloys (72 at.% Ru) that commonly form lamellae and inclusions in Pt–Fe alloy (Oberthür *et al.* 2004) (Fig. 1b). The presence of a Ru-rich alloy as an outermost rim around Ru-rich oxides or hydroxides suggests that the alloys formed by dehydration and reduction of these phases (Fig. 6a).

There are increasing data on Ru-rich oxides. Hey (1999) reported a Ru–Rh–Mn-"oxide" replacing laurite associated with Pt–Pd sulfide from the UG–2 chromitite. An unnamed Ru–Mn–Fe hydroxide of approximate composition $(Ru,Fe)_{0.75}Mn_{0.25}(O,OH)_3$ was described from a chromitite sample in the Pirogues mineralization, New Caledonia (Augé & Legendre 1994). Ru–Os–Ir–Fe oxides also are reported from altered and weathered chromitites in Alaskan-type, ophiolitic and stratiform occurrences (Garuti & Zaccarini 1997, Garuti *et al.* 1997, Milliotti 1994). The stoichiometries of the Ru oxide phases ranges between RuO_4 and Ru_2O_3, with values of the atomic ratio PGE:BM ranging from 5 to 1. In contrast to the Ru-rich "oxides" described in this paper, the chromitite-hosted examples have lower Rh, but higher Ir and Os. The "second rim" of Figure 6a best approaches those compositions reported by Garuti *et al.* (1997) from the Urals.

Alteration Phenomena in Rh Sulfide

Rh-rich thiospinel rims

Bowieite [Rh_2S_3] and miassite [$Rh_{17}S_{15}$] commonly occur in polyphase grains of Pt–Fe alloy. They are mostly unaltered; however, a narrow rim of Rh-rich thiospinel (cuprorhodsite) can be observed in a few cases, commonly in direct contact with porous Pt–Fe alloys (type 5.1, Table 3, Fig. 6b). In such cases, a thin zone of Pt-rich thiospinel (malanite) may be present.

Porous rim of Rh alloy

A porous Rh-rich alloy (90–92 wt.% Rh) is attached to, or coats Rh sulfides and aggregates of laurite plus Rh sulfide (type 5.2, Table 3). In one such case, textural features (desiccation cracks) of the Rh-rich phase suggest derivation from an Rh-rich precursor phase (Fig. 6c).

Other inclusions and coatings

Some PGM nuggets are intergrown with non-PGE phases that occur either as inclusions, pore fillings, or a complete or partial rim coating the nuggets. Minerals that have been identified include: halite, calcite and Mn-rich carbonate as inclusions in porous platinum (Pt–Pd–Ni sulfide alteration), actinolitic amphibole (7.7 Si *apfu*, Mg# 87) attached to porous Pt–Fe alloy, talc filling veinlets in Pt–Fe oxides (Fig. 4f), chlorite or smectite (or both) as a continuous rim (Figs. 4a, b), orthopyroxene ($En_{77}Fs_{20}Wo_3$) in porous platinum (Fig. 5b), and Fe oxides or hydroxides (Fig. 6a). Contents of SiO_2 in various layer silicates range from 33–40 wt.% (chlorite and smectite) to 58–61 wt.% (talc). The chlorite and smectite are Fe-rich (Mg# <30), Ca ranges from 0.5 to 3 wt.% CaO, and Mn, from 0.1 to 12 wt.% MnO.

A Pt–Fe alloy grain replaced by ferronickelplatinum and Pt-rich awaruite (Fig. 1e) is coated by a thin rind, 10–20 μm thick, of a Mn-bearing smectite intergrown with Fe–Mn-rich hydroxides. Some layer silicate

minerals included in porous platinum have appreciable concentrations of Pt (14–18 wt.% Pt; the contribution of surrounding PGE phases to these values is not clear, however). A probable smectite-like mineral coating a composite Pt–Fe alloy grain is Pd- and Mn-rich (3.6 wt.% Pd, 12 wt.% MnO), carries appreciable Ni, Cu and Ca (analysis 222, Fig. 6e), and is intergrown with a Pd-bearing impure Fe hydroxide phase, and a probable Pd oxide. Fe oxide or hydroxides (hematite, magnetite, goethite) have up to 0.44 wt.% Ru, 1.18% Rh, 1.58% Pd, 5% Ir and 4% Pt. Chromian spinel was observed in association with PGM only in two cases, notably with [Pt(Fe,Cu)] and a two-phase Pt–Fe alloy – laurite grain.

Discussion

The origin of Pt–Fe alloy, the most abundant PGM in most placers worldwide (Cabri *et al*. 1996, Weiser 2002), remains controversial. Textural and geochemical arguments, such as the presence of Ru–Ir–Os alloy lamellae and Os isotope compositions, are regarded by most researchers to indicate that many of the Pt–Fe grains originate from high-temperature (*i.e.,* magmatic) processes (*e.g.,* Cabri *et al*. 1996, Weiser 2002, Malitch & Thalhammer 2002).

Some authors have proposed a secondary origin of PGM in placers and soils (Augusthitis 1965, Bowles 1986, 1990, 1995, Ottemann & Augusthitis 1967, Stumpfl 1974). Cousins (1973) and Cousins & Kinloch (1976) pointed out that size, shape, composition and microtexture of many eluvial and alluvial PGM differ from those observed in bedrocks and ores. They proposed formation of secondary PGM due to a simplified process. Serpentinization or weathering results in decomposition of base-metal sulfides carrying PGE in solid solution, and the PGE are removed and transported as colloidal particles. Such particles may coalesce or accrete to form larger particles and aggregates of alloy. Textures such as zoning, reniform and mammillary textures are considered evidence for accretion and secondary growth in a low-temperature environment (Stumpfl 1974). Unconstrained three-dimensional growth, corrosion features on mineral faces, overplating of mineral faces, colloform and cyclic zonation, porous and spongy Pt–Fe nuggets, and overgrowths of one phase by another were considered unique to hydrothermal and supergene processes of formation (Bowles 1995).

Cabri & Harris (1975) disputed a supergene origin of PGM as proposed by Augusthitis (1965), and Cabri *et al*. (1996) cited only two likely exceptions where Pt nuggets may have formed in a surficial environment, namely palladian gold, potarite and native platinum in alluvial sediments from Devon, England, and botryoidal, zoned Pt–Pd nuggets from the Bom Sucesso stream in Brazil. The Brazilian example has been critically evaluated by Fleet *et al*. (2002), who concluded that the alluvial PGM most likely originated from detrital grains that crystallized from low-temperature hydrothermal fluids. In their study of gold and PGM (isoferroplatinum and Os–Ir alloy) in offshore placers near Goodnews Bay, Alaska, Mardock & Barker (1991) found textures related to both derivation of PGM grains from mechanically weathered primary ore (*i.e.,* typical assemblages of inclusions, exsolution phenomena) and subsequent accretion (*i.e.,* microcrystalline assemblages of PGM in grain-rim cavities, suggesting leaching and crystallization). This important observation pertains to many occurrences of placer PGM; therefore, a combination of primary and secondary processes has to be considered to explain textural and chemical attributes of PGM nuggets.

A further point tackled in the following discussion is the formation of PGE "oxides" and "hydroxides" (for simplicity referred to as "oxides" in the following). Convincing evidence of their presence has been presented by a number of authors (Augé & Legendre 1992, 1994, Barkov *et al*. 1999, Cabral *et al*. 2001, 2002, 2004, Cabri *et al*. 1996, Evans & Spratt 2000, Evans 2002, Garuti & Zaccarini 1997, Garuti *et al*. 1997, Hey 1999, Jedwab *et al*. 1993, Jedwab 1995, 2004, McDonald *et al*. 1999a, b, Milliotti & Stumpfl 1993, Milliotti 1994, Moreno *et al*. 1999, Ortega *et al*. 2004, Tolstykh *et al*. 2000, Weiser 1990). Thorough mineralogical characterization of such minerals is generally difficult because of their small grain-size, common intergrowth with primary phases, ubiquitous porosity, nonstoichiometry, and analytical problems. According to the above references, the number of potential PGE oxides is large. It includes combinations of oxygen with all PGE, iron, manganese, the base metals Cu, Ni and Co and, in some cases, As, Sb, Bi, Te, Hg, Pb and Au. Concentrations of Si, Al, Mg, Ti, Ca, Na, K and Cl have been reported from a few occurrences only. The presence of hydrogen was confirmed using micro-ERDA in a microcracked Pd–O phase associated with gold from Gongo Soco (Cabral *et al*. 2004). Two modes of formation are discussed for PGE oxides: (i) crystallization and neoformation under lateritic conditions in soils and in placers, probably by precipitation from solutions, and (ii) alteration, *i.e.,* oxidation, of PGM precursor minerals. The conditions of formation are agreed to be low temperature, but different opinions exist about the predominance of surficial or hydrothermal processes. In some occurrences, PGE oxides clearly are not supergene minerals, and are related to low-temperature hydrothermal alteration of PGM involving deuteric fluids (Barkov *et al*. 1999, Tolstykh *et al*. 2000). In others, PGE oxides appear to have directly precipitated from hydrothermal solutions. McDonald *et al*. (1999b) reported Pt oxides (PtO and PtO_2) from the Waterberg, South Africa, hydrothermal platinum deposit and suggested formation from low-salinity acidic hydrothermal solutions at 200–300°C, and later transformation into Pt and Pt–Pd alloys. In

other instances, the PGE oxide grains are believed to be of supergene origin, *e.g.,* from gossans (Ortega *et al*. 2004) and weathered chromitite (Milliotti 1994, Hey 1999).

In the following discussion, the more abundant alteration-related features of PGM grains and aggregates from alluvial sediments in the Eastern Bushveld Complex are treated in terms of possible processes of formation, from higher temperature and reducing, to lower temperature and oxidizing environments (Table 8).

Sulfidation of PGE alloys: magmatic–hydrothermal processes?

Several PGM grains have a narrow rim of sulfide. Examples include cooperite mantling Pt–Fe alloy, PdS (vysotskite) mantling braggite, and Rh–Pt-rich thiospinel mantling Rh sulfides (Table 3, Fig. 6b). The epitactic overgrowth of PtS on an altered surface of Pt–Fe alloy has been illustrated by Bowles (1995) and attributed to secondary growth. Evstigneeva *et al*. (1995) demonstrated the replacement of Pt–Fe alloy by PtS under reducing hydrothermal conditions (~ 240°C, P_{total} ≈ 300 bar). We suggest that sulfidation of PGE alloys most likely reflects a late magmatic or hydrothermal formation. Sulfidation curves for Pt minerals were summarized by Makovicky (2002) in the temperature range from 500 to 1200°C; the pairs Pt–PtS, Pt_3Fe–PtS and PtS–$CuPt_2S_4$ reflect increasing sulfur fugacities at a given temperature [*e.g.,* for 600°C from log $f(S_2)$ values of –7 for Pt–PtS to –4 for PtS–$CuPt_2S_4$]. The thiospinel phase is stable between 900 and 510°C in the system Cu–Rh–S, whereas it disappears at 500°C (Makovicky 2002). Pt- and Rh-rich thiospinel is common in primary magmatic and secondary (placer) deposits worldwide (Melcher 2000), and there is accumulating evidence for its omnipresence in the UG–2 and other chromitites of the Bushveld Complex (Merkle 1998, Hey 1999, Penberthy & Merkle 1999, Cawthorn *et al*. 2002a).

TABLE 8. PROPOSED SEQUENCE OF EVENTS PRODUCING ZONED AND ALTERED PGM IN PLACERS OF THE EASTERN BUSHVELD COMPLEX

Event	Magmatic	Late magmatic	Serpentinization	Hydrothermal	Weathering	Placer environment
Eh	reducing	reducing	reducing	intermediate	oxidizing	oxidizing
$f(S_2)$	high	moderate	low	low	low	low
pH	low	low	low	low	3-5	neutral
T°C	>700	700 > T > 400	400 > T > 200	200 > T > 100	ambient	ambient
Type (Table 3)						
1 (1.1, Ni)	Pt_3Fe	Pt_2NiFe	Ni_2PtFe			Pd_3Pb, Fe oxide
1 (1.2, Cu)	Pt_3Fe	Pt_2CuFe	Pt_2CuFe	Pt		Pd_3Pb
1 (porous)	Pt_3Fe	$Pt(Cu,Fe)$			leaching	
1 (1.4, ox)	Pt_3Fe	$Pt(Cu,Fe)$		Pt-Fe ox?	Pt-Fe ox	Pt-Fe-SiO_2
2 (Pt-Pd sulfide)	(Pt,Pd)S	(PdS)		Pt-ox?, Pt	Pt	Pt
3 (Sperrylite)	$PtAs_2$			Pt-ox?, Pt	Pt	Pt
4 (Laurite)	RuS_2			RuO_2	RuO_2, Ru	Ru
5 (Rh sulfide)	Rh_2S_3	$CuRh_2S_4$		RhO_2?	RhO_2, Rh	Rh

Oxide formulae are simplified and generalized. The relative conditions of crystallization and modification (Eh, sulfur fugacity, pH and temperature) are estimated from mineral assemblages.

Alteration of Pt–Fe alloy to Pt–Fe–Ni–Cu alloys: moderate temperature, reducing environment

This group of textures includes those where Pt–Fe alloys are modified owing to formation of base-metal-rich alloy phases [Pt(Ni,Fe,Cu)]. There is no evidence that oxidation has played a role in their formation. A two-stage process of alteration is observed in a number of Pt–Fe alloy grains: (1) formation of an inner rim of ferronickelplatinum, and (2) later formation of an outer rim of Pt-bearing Ni–Fe alloy, according to the following generalized reactions:

$$2\ Pt_3Fe + 3\ NiO + 13\ FeO = 3\ Pt_2NiFe + 4\ Fe_3O_4$$

$$Pt_2NiFe + 3\ NiO + 13\ FeO = 2\ Ni_2PtFe + 4\ Fe_3O_4$$

Formation of increasingly more Ni-rich alloy from Pt-rich alloy is probably controlled by infiltration processes within grains. Some of the altered grains are porous, but the additional presence of oxygen could not be demonstrated.

Pt-bearing Ni–Fe alloy as a decomposition product of Pt–Fe alloy is described here for the first time. The chemical composition of the Ni–Fe–Pt phase, though variable, points to the presence of Pt-bearing awaruite. Elsewhere, PGE-rich awaruite is exclusively associated with alteration and serpentinization processes affecting chromitite (Ahmed & Bevan 1981, Corrivaux & Laflamme 1990, Kieser 1994, Tarkian *et al*. 1996). The formation of awaruite [Ni_3Fe] is commonly linked to serpentinization processes (Ramdohr 1967, Eckstrand 1975, Stockman & Hlava 1984, Frost 1985), which are characterized by extremely low $f(S_2)$ and $f(O_2)$ conditions. With these constraints, the alteration of Pt–Fe alloy to Ni-rich Pt alloy may be attributed to a late-stage magmatic-hydrothermal phase, possibly concomitant with serpentinization down to lower temperatures. Nickel could have been released by the hydration of olivine (*e.g.,* Mg–Fe–Ni olivine + NaOH-bearing fluid = serpentine + brucite + Ni-rich magnetite + awaruite: Filippidis 1985) or breakdown of magmatic Fe–Ni sulfide.

In a similar way, tetraferroplatinum and tulameenite are found commonly to replace grains of Pt–Fe alloy (Figs. 2b, 3a–f, 4a–d). The association of Pt–Fe alloy with [Pt(Fe,Cu)] is common in both placer deposits

and in primary deposits that underwent postmagmatic hydrothermal alteration (Kieser 1994). The presence of Cu in secondary Pt–Fe alloy probably reflects the greater mobility of Cu released by the alteration of base-metal sulfides during serpentinization, compared with Fe and Ni (Kieser 1994). Inclusions found in the Cu-rich assemblage differ from those in the Ni-rich assemblage. This might indicate either a different source for the Cu-rich assemblage (a source relatively rich in base-metal sulfdes, *e.g.,* the Merensky Reef), or different postmagmatic histories, *e.g.,* hydrothermal alteration *versus* serpentinization.

Delicate textures preserved in some "Ni-altered" grains point to minimal mechanical transport. The formation of Pt–Fe–Ni–Cu alloys in an oxidizing environment is considered unlikely. However, exposure to surface fluids may have created porosity, triggering the local oxidation of detrital grains. Precipitation of [Pd_3Pb] and other minerals from migrating fluids carrying Pd and Rh in solution may reflect processes acting during weathering or after deposition.

Oxidation of PGE sulfides: low-temperature, oxidizing environment

PGM grains in this group show direct or indirect evidence of oxidation. This includes formation of native platinum from PGE sulfides and arsenides, and formation of PGE oxides. Cooperite and braggite, the most common sulfides encountered in the concentrates, are commonly coated by a porous rim of native platinum (Figs. 5a–d). Although rarely coated by platinum, sperrylite may show similar textures, and in one case (Fig. 5f), an oxygen-bearing intermediate Pt-(Fe) phase was identified. Formation of PGE metal by oxidation of PGE sulfides may follow simplified reactions as:

$$PtS + 3/2\ O_2 + H_2O = Pt^0 + SO_4^{2-} + 2\ H^+$$

$$RuS_2 + 3\ O_2 + 2\ H_2O = Ru^0 + 2\ SO_4^{2-} + 4\ H^+$$

In both reactions, sulfur is oxidized to sulfate, whereas the PGE are reduced to metals. The fugacity of oxygen is controlled by Fe hydroxides, which are common in the alteration rims. On the other hand, platinum alloys crystallize under low fugacity of sulfur and low-temperature conditions from hydrothermal solutions (Evstigneeva *et al*. 1995, Evstigneeva & Tarkian 1996). These authors proposed the following reaction to transform PtS into Pt under hydrothermal conditions (400°C):

$$2\ PtS + C + 3H_2O = 2\ Pt^0 + H_2CO_3 + 2\ H_2S$$

Laurite is replaced by Ru-rich oxides or hydroxides (or both) of variable stoichiometry that subsequently are rimmed by Ru alloy (Fig. 6a), probably following reactions such as:

$$RuS_2 + 4\ O_2 + 2\ H_2O = RuO_2 + 2\ SO_4^{2-} + 4\ H^+$$

$$RuO_2 = Ru^0 + O_2$$

The following PGE-bearing oxides are identified in the present study: (i) Ru–Rh-rich oxides, (ii) Pt–Fe-rich oxides, (iii) Pd-rich oxides, and (iv) Fe oxide or hydroxide with minor to trace PGE. (i) Ru- and Rh-rich oxides of probable RuO_2 to RuO stoichiometry are observed in two cases, one being clearly related to decomposition or desulfurization of laurite (Fig. 6a). Similar minerals are reported from altered chromitites (Garuti & Zaccarini 1997, Garuti *et al*. 1997). (ii) Porous Pt–Fe oxide grains with appreciable concentrations of Si, Al, and Mg may have formed from Pt–Fe alloy and Pt(Fe,Cu) (Figs. 2c, 4e–f), as indicated by values of the PGE:BM ratio intermediate between 2.1 and 0.9 (Fig. 8a). The metal:oxygen ratio varies widely, from >10 to 0.6. Grains of similar composition were described from weathered bedrock and placers in New Caledonia (Augé & Legendre 1994), from the weathered Main Sulphide Zone, Great Dyke, Zimbabwe (Evans & Spratt 2000), and from placer occurrences in Burma and Ecuador (Cabri *et al*. 1996). (iii) Pd-rich oxygen-bearing phases are rare in the PGM grains studied. A few narrow grains of Pd oxide and Pd-rich smectite (3.6 wt.% Pd) were identified in one nugget (Fig. 4a). The composition of the Pd oxide is similar to "palladinite" [PdO] from Itabira (Jedwab *et al*. 1993), and to [PdO] or [$Pd(OH)_2$] described from shallow levels of an ultramafic intrusion in Madagascar (McDonald *et al*. 1999a). Pd–O–H phases with a metal:oxygen ratio between 1 and 3 have also been reported from hydrothermal vein-type Au–Pd–Pt deposits in Brazil (Cabral *et al*. 2001, 2002, 2004). Relative to associated goethite, the Pd–O–H compound is metastable and deficient in oxygen, giving rise to native palladium *via* a deoxygenation–dehydration process. (iv) Pt–Fe alloy and tetraferroplatinum-tulameenite nuggets occasionally have a rim of Fe hydroxides and oxides that may carry up to several weight percent PGE, *e.g.,* 5 wt.% Ir, 4% Pd and 4% Pt. PGE-rich goethite carrying up to 20 wt.% Ru and 12 wt.% Pt has been reported as an alteration product in chromitite from Brazil (Milliotti 1994).

The combined textural and geochemical evidence indicates that Pt–Pd sulfides, laurite and sperrylite are first oxidized to oxide–hydroxide phases that later decompose to form native metal phases. The porosity observed in many altered grains points to a phase transformation, involving volume reduction, from a precursor PGE alloy or sulfide phase into a metallic PGE phase *via* PGE oxide or hydroxides. Stockman & Hlava (1984) suggested that the formation of a porous Ru-rich alloy from laurite involves desulfurization of laurite after formation of cracks exposing them to reducing conditions, and subsequent addition of Fe and Ni under high activities of Fe and Ni. The volume change resulting from decomposition of laurite is of the order

of 30–40%, which explains the considerable porosity in the products.

Hey (1999) identified oxygen-bearing phases in weathered UG–2 chromitite and suggested that they formed by *in situ* weathering processes. We propose that formation of the various PGE-bearing oxides found in the placer inventory is mainly restricted to surface exposure in zones of weathering of bedrock and placers, and that some of the PGE-bearing goethite and smectite most likely formed during weathering within the placer environment. However, aqueous fluids may also affect pre-existing PGM, resulting in occasional *in situ* neoformation of PGE oxides, which may be liberated as grains from their source rocks and deposited within placers.

The Maandagshoek placer PGM assemblage: sources and processes

The morphological and sedimentological history of the north–south-directed valley hosting the alluvial PGM in the Eastern Bushveld Complex is poorly constrained. Cawthorn (2001) suggested that the formation of the initial valley was the result of glacial activity in a mountainous terrain during Permo-Carboniferous glaciation, and that sediments deposited in the valley since have been eroded to the original glacial morphology.

The diversity of PGM assemblages and alteration features suggests that the various PGM grains record various origins and complex histories. Cawthorn *et al.* (2002a, b) commented that the considerable lateral mineralogical variation within the PGE reefs does not facilitate correlation. Delicate textures preserved in many PGM grains probably prohibit extended transport, indicating nearby sources. Oberthür *et al.* (2004) discussed possible sources of the grains, with contributions from the Merensky Reef, the UG–2 and other chromitites, and the platiniferous dunite pipes outcropping in the area. Assemblages of primary PGM in these deposits differ in grain size and mineralogy; for example, PGM in the Merensky Reef are generally coarser than in the UG–2. Laurite and Pt–Fe alloy, followed by Pt–Pd–Ni sulfide, dominate in the UG–2 reef at Union Section (Hey 1999). Pt–Fe alloy, followed by geversite, sperrylite and sulfarsenides, and the conspicuous absence of sulfides, are characteristic of the platiniferous dunite pipes (Tarkian & Stumpfl 1975). A Ru-rich alloy was described from chromitite xenoliths in platiniferous pipes (Zaccarini *et al.* 2002) and the UG–1 chromitite (Merkle 1998). Taking the proximity to the pipes into account, grains of Pt–Fe alloy associated with Ru alloy may probably have originated from them. Serpentinization of dunitic pipes would also provide a source of Ni with which to form secondary ferronickelplatinum (Cabri *et al.* 1977) and Ni-rich Pt alloys, forming a concentric rim around Pt–Fe alloy and Ru alloy grains (Fig. 1b). At lower temperatures during serpentinization, Pt-rich awaruite may have formed under reducing conditions. Although concentric textures and porosity suggest *in situ* alteration at ambient conditions, formation of Ni-rich Pt–Fe alloy after transport, during diagenesis at low temperature, appears less probable owing to the difficulty to envisage the necessary reducing conditions in the sedimentary deposits of the Bushveld Complex.

Recent studies on weathered sulfide-rich PGE reefs along the Great Dyke, Zimbabwe, have shown that Pt-(Fe) alloy phases, along with PGE oxides, preferentially form at the expense of primary PGE bismuthotellurides, and probably sulfides as well, whereas sperrylite remains stable (Evans *et al.* 1994, Oberthür *et al.* 2003, Gregor 2004, Oberthür & Melcher 2005). However, grain sizes of many of these neoformations are small, in the 1 to 20 μm range, and demonstrable proof of the nucleation of nugget-sized grains in the 0.1 to 1 mm range within oxidized ores and soils is lacking. At the Mimosa mine, Zimbabwe, Pt- and Pd-bearing base-metal sulfides, present as interstitial sulfide droplets 100–200 μm in size, weather to PGE-bearing goethite (Gregor 2004). With respect to the Bushveld Complex, Hey (1999) has demonstrated that weathering in the UG–2 reef leads to the destruction of base-metal sulfides, and that many PGM show features of decomposition and alteration, some of which are similar to those found in the placer assemblage.

Following these lines of evidence, the most likely scenario to account for the textural and mineralogical features observed in the alluvial PGE placer deposits of the Eastern Bushveld Complex comprises (i) different sources of the PGM grains, (ii) variable degrees of late-magmatic to hydrothermal alteration, and (iii) weathering affecting those sources. The PGM liberated from fresh, altered and weathered sources, mainly in the Critical Zone of the Bushveld, have accumulated in the placers. An unknown portion of PGE, especially Pd and Rh, originally concentrated in base-metal sulfides, was redistributed to form phases overgrowing or replacing detrital grains. Evidence for significant crystallization or growth of Pt–Fe alloys after transport is lacking; rather, such phases have been leached (porous grains), or transformed into metallic phases and PGE oxides.

Conclusions

Investigation of PGM grains from alluvial placers in the Eastern Bushveld Complex reveals the following characteristics, summarized in Table 8. About 32% of the 790 PGM grains investigated show attributes of modification or alteration. Grains of Pt–Fe alloy are most susceptible to such processes, followed by cooperite–braggite. In our opinion, different processes are indicated by three groups of textures.

1. Postmagmatic, fluid-assisted hydrothermal modification at elevated fugacity of sulfur [*i.e.,* rim of PtS on Pt_3Fe, rim of PdS on (Pt,Pd,Ni)S].

2. Modification at reducing conditions: concentric replacement of Pt–Fe alloy by tetraferroplatinum–tulameenite, also associated with Pd–(Te–Sb–Sn) phases and gold, is probably related to late-magmatic processes. Some grains of Pt–Fe alloy are coated by ferronickelplatinum and an outer rim of Pt-bearing Ni–Fe alloy (Pt-rich awaruite). The restricted paragenesis of the host Pt–Fe alloy with lamellae of Ru-rich alloy and the lack of sulfides point to a unique source, possibly from nearby platiniferous dunite pipes. Alteration took place under reducing conditions, most likely during serpentinization of the protolith.

3. Modification at oxidizing conditions: (i) Pt–Fe alloy or Pt(Fe,Cu) precursor phases are replaced by inhomogeneous Pt–Fe oxide phases having variable PGE:BM and metal:oxygen ratios. (ii) Replacement of laurite by Ru-rich oxides or hydroxides. Metallic elements (Ru, Rh) around altered grains probably formed from dehydration and reduction of PGE-rich oxide or hydroxide as precursor phases. (iii) Replacement of Pt–Pd–Ni sulfides (cooperite–braggite) and sperrylite by native platinum or Pt–Pd alloy displaying a spongy texture, inclusions of Fe-rich phases and thin rims of homogeneous platinum. Environments favoring the formation of metallic elements from sulfides range from hydrothermal in bedrock to *in situ* weathering, to precipitation of platinum from fluids after sedimentation in placers. We contend that weathering is the dominant process. Minor to trace concentrations of PGE in secondary phases such as Fe oxide and hydroxide, chlorite and smectite forming a continuous rim around PGM grains are considered to have formed *in situ* within the placer deposits.

Acknowledgements

Many thanks to Grant Cawthorn for ably guiding us in the field, and to Anglo Platinum for allowing access to their property. Lothar Gast and Christian Wöhrl produced the concentrates both in the field and laboratory and performed extensive SEM studies. Gilles Laflamme of CANMET provided excellent polished sections of the single PGM grains. Ronald Bakker (Department of Applied Geosciences and Geophysics, University of Leoben) assisted with Raman spectroscopy. Discussions with Thomas Meisel (Leoben) are greatly appreciated. Thanks to Associate Editor Jim Mungall and the reviewers Mike Fleet and Mike Zientek for their encouraging comments and much positive input. The authors dedicate this publication to Michael E. Fleet on the occasion of his retirement, and to the late Eugen F. Stumpfl (1931–2004). Both have significantly contributed to our present understanding of processes of formation of platinum-group-element deposits.

References

Ahmed, Z. & Bevan, J.C. (1981): Awaruite, iridian awaruite, and a new Ru–Os–Ir–Ni–Fe alloy from the Sakhakot–Quila complex, Malakand agency, Pakistan. *Mineral. Mag.* **44**, 225-230.

Augé, T., & Legendre, O. (1992): Pt–Fe nuggets from alluvial deposits in eastern Madagascar. *Can. Mineral.* **30**, 983-1004.

_____ & _____ (1994): Platinum-group element oxides from the Pirogues ophiolitic mineralization, New Caledonia: origin and significance. *Econ. Geol.* **89**, 1454-1468.

Augusthitis, S.S. (1965): Mineralogical and geochemical studies of the platiniferous dunite – birbirite – pyroxenite complex of Yubdo, Birbir, W. Ethiopia. *Chem. Erde* **24**, 159-165.

Barkov, A.Y., Halkoaho, T.A.A., Roberts, A.C., Criddle, A.J., Martin, R.F. & Papunen, H. (1999): New Pd–Pb and Pb–V oxides from a bonanza-type PGE-rich, nearly BMS-free deposit in the Penikat layered complex, Finland. *Can. Mineral.* **37**, 1507-1524.

Bowles, J.F.W. (1986): The development of platinum-group minerals in laterites. *Econ. Geol.* **81**, 1278-1285.

_____ (1990): Platinum–iron alloys, their structural and magnetic characteristics in relation to hydrothermal and low-temperature genesis. *Mineral. Petrol.* **43**, 37-47.

_____ (1995): The development of platinum-group minerals (PGM) in laterites: mineral morphology. *Chron. rech. minières* **520**, 55-63.

_____, Gize, A.P. & Cowden, A. (1994): The mobility of the platinum-group elements in the soils of the Freetown Peninsula, Sierra Leone. *Can. Mineral.* **32**, 957-967.

Cabral, A.R., Lehmann, B., Grambole, D. & Herrmann, F. (2004): Hydrogen in a natural Pd–O compound from Gongo Soco, Minas Gerais, Brazil. *Can. Mineral.* **42**, 689-694.

_____, _____, Kwitko, R., Jones, R.D., Pires, F.R.M., Rocha Filho, O.G. & Innocentini, M.D. (2001): Palladium-oxygenated compounds of the Gongo Soco mine, Quadrilátero Ferrífero, central Minas Gerais, Brazil. *Mineral. Mag.* **65**, 169-179.

_____, _____, Kwitko-Ribeiro, R. & Cravo Costa, C.H. (2002): Palladium and platinum minerals from the Serra Pelada Au–Pd–Pt deposit, Carajás mineral province, northern Brazil. *Can. Mineral.* **40**, 1451-1463.

Cabri, L.J. & Harris, D.C. (1975): Zoning in Os–Ir alloys and the relation of the geological and tectonic environment of the source rocks to the bulk Pt:Pt + Ir + Os ratio for placers. *Can. Mineral.* **13**, 266-274.

_____, _____ & WEISER, T. (1996): Mineralogy and distribution of platinum-group mineral (PGM) placer deposits of the world. *Explor. Mining Geol.* **5**, 73-167.

_____, ROSENZWEIG, A. & PINCH, W.W. (1977): Platinum-group minerals from Onverwacht. I. Pt–Fe–Cu–Ni alloys. *Can. Mineral.* **15**, 380-384.

CAWTHORN, R.G. (1999): The discovery of the platiniferous Merensky Reef in 1924. *S. Afr. J. Geol.* **102**, 178-183.

_____ (2001): A stream sediment geological re-investigation of the discovery of the platiniferous Merensky Reef, Bushveld Complex. *J. Geochem. Explor.* **72**, 59-69.

_____, LEE, C.A., SCHOUWSTRA, R.P. & MELLOWSHIP, P. (2002b): Relationship between PGE and PGM in the Bushveld Complex. *Can. Mineral.* **40**, 311-328.

_____, MERKLE, R.K.W. & VILJOEN, M.J. (2002a): Platinum-group element deposits in the Bushveld Complex, South Africa. *In* The Geology, Geochemistry, Mineralogy and Mineral Beneficiation of Platinum-Group Elements (L.J. Cabri, ed.). *Can. Inst. Mining, Metall. Petroleum, Spec. Vol.* **54**, 389-429.

CORRIVAUX, L. & LAFLAMME, J.H.G. (1990): Minéralogie des éléments du groupe du platine dans les chromitites de l'ophiolite de Thetford Mines, Québec. *Can. Mineral.* **28**, 579-595.

COUSINS, C.A. (1973): Platinoids of the Witwatersrand system. *J. S. Afr. Inst. Mining Metall.* **73**, 184-199.

_____ & KINLOCH, E.D. (1976): Some observations on textures and inclusions on alluvial platinoids. *Econ. Geol.* **71**, 1377-1398.

ECKSTRAND, O.R. (1975): The Dumont serpentinite: a model for control of nickeliferous opaque mineral assemblages by alteration reactions in ultramafic rocks. *Econ. Geol.* **70**, 183-201.

EVANS, D.M. (2002): Potential for bulk mining of oxidized platinum-group element deposits. *Trans. Inst. Mining Metall., Sect. B: Appl. Earth Sci.* **111**, 81-86.

_____, BUCHANAN, D.L. & HALL, G.E.M. (1994): Dispersion of platinum, palladium and gold from the Main Sulphide Zone, Great Dyke, Zimbabwe. *Trans. Inst. Mining Metall., Sect. B: Appl. Earth Sci.* **103**, 57-67.

_____ & SPRATT, J. (2000): Platinum and palladium oxides/hydroxides from the Great Dyke, Zimbabwe, and thoughts on their stability and possible extraction. *In* Applied Mineralogy (D. Rammlmair, D. *et al.*, eds.). Balkema, Rotterdam, The Netherlands (289-292).

EVSTIGNEEVA, T.L., MOH, G.H. & TARKIAN, M. (1995): Hydrothermal recrystallization of PGE- and Fe–Ni-sulfide assemblages. *Neues Jahrb. Mineral., Abh.* **149**, 273-277.

_____ & TARKIAN, M. (1996): Synthesis of platinum-group minerals under hydrothermal conditions. *Eur. J. Mineral.* **8**, 549-564.

FILLIPPIDIS, A. (1985): Formation of awaruite in the system Ni–Fe–Mg–Si–O–H–S and olivine hydration with NaOH solution, an experimental study. *Econ. Geol.* **80**, 1974-1980.

FLEET, M.E., DE ALMEIDA, C.M. & ANGELI, N. (2002): Botryoidal platinum, palladium and potarite from the Bom Sucesso stream, Minas Gerais, Brazil: compositional zoning and origin. *Can. Mineral.* **40**, 341-355.

FROST, B.R. (1985): On the stability of sulphides, oxides, and native metals in serpentinite. *J. Petrol.* **26**, 31-63.

GARUTI, G. & ZACCARINI, F. (1997): In situ alteration of platinum-group minerals at low temperature: evidence from serpentinized and weathered chromitite of the Vourinos complex, Greece. *Can. Mineral.* **35**, 611-626.

_____, _____, CABELLA, R. & FERSHTATER, G. (1997): Occurrence of unknown Ru–Os–Ir–Fe oxides in the chromitites of the Nurali ultramafic complex, southern Urals, Russia. *Can. Mineral.* **35**, 1431-1439.

GAST, L. & WITTICH, C. (2001): Detritische Platingruppenminerale im Eastern Bushveld, Republik Südafrika – Eine Reconnaisance-Beprobung. *Archive of the Bundesanstalt für Geowissenschaften und Rohstoffe* (*BGR, Hannover*), *Archive-No.* **0120650**.

GREGOR, S. (2004): Evaluation of PGE mineralization in the oxidized Main Sulfide Zone at Mimosa mine, Great Dyke, Zimbabwe. *Archive of the Bundesanstalt für Geowissenschaften und Rohstoffe (BGR, Hannover), Internal File* **10478/04**.

HANSEN, M. & ANDERKO, K. (1958): *Constitution of Binary Alloys* (2nd ed.). McGraw-Hill, New York, N.Y.

HEY, P.V. (1999): The effects of weathering on the UG–2 chromitite reef of the Bushveld Complex, with special reference to the platinum-group minerals. *S. Afr. J. Geol.* **102**, 251-260.

JEDWAB, J. (1995): Oxygenated platinum-group element and transition-metal (Ti, Cr, Mn, Fe, Co, Ni) compounds in the supergene domain. *Chron. rech. minières* **520**, 47-53.

_____ (2004): "Irite" (Hermann, 1836/1841) from the Urals. *Mineral. Mag.* **68**, 369-394.

_____, CASSEDANNE, J., CRIDDLE, A.J., DU RY, P., GHYSENS, G., MEISSER, N., PIRET, P. & STANLEY, C.J. (1993): Rediscovery of palladinite PdO from Itabira (Minas Gerais, Brazil) and from Ruwe (Shaba, Zaire). IAGOD, Int. Symp. on Mineralization Related to Mafic and Ultramafic Rocks (Orléans). *Terra Nova* **5**, *Abstr. Suppl.* 3, 22.

KIESER, N.B.J. (1994): In-situ modification of platinum-group minerals in Tonsina ultramafic complex, south-central Alaska: implications for surficial dispersion and geochemi-

cal exploration. *Trans. Inst. Mining Metall., Sect. B: Appl. Earth Sci.* **103**, 45-52.

MAKOVICKY, E. (2002): Ternary and quaternary phase systems with PGE. *In* The Geology, Geochemistry, Mineralogy and Mineral Beneficiation of Platinum-Group Elements (L.J. Cabri, ed.). *Can. Inst. Mining, Metall. Petroleum, Spec. Vol.* **54**, 131-175.

MALITCH, K.N. & THALHAMMER, O.A.R. (2002): Pt–Fe nuggets from clinopyroxenite–dunite massifs, Russia: a structural, compositional and osmium-isotope study. *Can. Mineral.* **40**, 395-417.

MARDOCK, C.L. & BARKER, J.C. (1991): Theories on the transport and deposition of gold and PGM minerals in offshore placers near Goodnews Bay, Alaska. *Ore Geol. Rev.* **6**, 211-227.

MCDONALD, I., OHNENSTETTER, D., OHNENSTETTER, M. & VAUGHAN, D.J. (1999a): Palladium oxides in ultramafic complexes near Lavatrafo, western Andriamena, Madagascar. *Mineral. Mag.* **63**, 345-352.

_____, _____, ROWE, J.P., TREDOUX, M., PATTRICK, R.A.D. & VAUGHAN, D.J. (1999b): Platinum precipitation in the Waterberg deposit, Naboomspruit, South Africa. *S. Afr. J. Geol.* **102**, 184-191.

MELCHER, F. (2000): Base metal – platinum- group element sulfides from the Urals and the Eastern Alps: characterization and significance for mineral systematics. *Mineral. Petrol.* **68**, 177-211.

MERENSKY, H. (1924): The various platinum occurrences on the farm Maandagshoek No. 148. Unpubl. memorandum to the Lydenburg Platinum Syndicate. Archives of the Merensky Trust, Duivelskloof, South Africa.

_____ (1926): Die neuentdeckten Platinfelder im mittleren Transvaal und ihre wirtschaftliche Bedeutung. *Z. Deutsch. Geol. Gesells.* **78**, 298-314.

MERKLE, R.K.W. (1998): Proportions of magmatic platinum-group minerals and evolution of mineralizing processes, UG–1 chromitite layer, Bushveld Complex. *In* International Platinum (N.P. Laverov & V.V. Distler, eds.). Theophrastos Publications, St. Petersburg, Russia (43-53).

MILLIOTTI, C.A. (1994): *Chromite and Platinum Mineralization at Morro Feio and Niquelandia, Brazil*. Ph.D. thesis, Mining University Leoben, Leoben, Austria.

_____ & STUMPFL, E.F. (1993): Platinum-group mineral inclusions, textures and distribution in the chromitites of the Niquelandia complex, Brazil. *In* Brazilian PGE Meeting (H. Jost & D. Macedo, eds.). Extended Abstr. Vol., 33-35.

MORENO, T., PRICHARD, H.M., LUNAR, R., MONTERRUBIO, S. & FISHER, P. (1999): Formation of a secondary platinum-group mineral assemblage in chromitites from the Herbeira ultramafic massif in Cabo Ortegal, NW Spain. *Eur. J. Mineral.* **11**, 363-378.

OBERTHÜR, T. & MELCHER, F. (2005) Behavior of PGE and PGM in the supergene environment: a case study of persistence and redistribution in the Main Sulfide Zone of the Great Dyke, Zimbabwe. *In* Exploration for Platinum-Group Element Deposits (J.E. Mungall, ed.). *Mineral. Assoc. Can., Short Course Vol.* **35**, 97-111.

_____, _____, GAST, L., WÖHRL, C. & LODZIAK, J. (2004): Detrital platinum-group minerals in rivers draining the eastern Bushveld Complex, South Africa. *Can. Mineral.* **42**, 563-582.

_____, WEISER, T. W., GAST, L. & KOJONEN, K. (2003): Geochemistry and mineralogy of the platinum-group elements at Hartley platinum mine, Zimbabwe. 2. Supergene redistribution in the oxidized Main Sulfide Zone of the Great Dyke, and alluvial platinum-group minerals. *Mineral. Deposita* **38**, 344-355.

ORTEGA, L., LUNAR, R., GARCÍA-PALOMERO, F., MORENO, T., MARTÍN-ESTÉVEZ, J.R., PRICHARD, H.M. & FISHER, P.C. (2004): The Aguablanca Ni–Cu–PGE deposit, southwestern Iberia: magmatic ore-forming processes and retrograde evolution. *Can. Mineral.* **42**, 325-350.

OTTEMANN, J. & AUGUSTHITIS, S.S. (1967): Geochemistry and origin of "platinum-nuggets" in laterite covers from ultrabasic rocks and birbirites of W. Ethiopia. *Mineral. Deposita* **1**, 269-277.

PENBERTHY, C.J. & MERKLE, R.K.W. (1999): Lateral variations in the platinum-group element content and mineralogy of the UG–2 chromitite layer, Bushveld Complex. *S. Afr. J. Geol.* **102**, 240-250.

RAMDOHR, P. (1967): A widespread mineral association, connected with serpentinization. *Neues Jahrb. Mineral., Abh.* **107**, 241-265.

SHUNK, F.A. (1969): *Constitution of Binary Alloys* (2nd Suppl.). McGraw-Hill, New York, N.Y.

STOCKMAN, H.W. & HLAVA, P.F. (1984): Platinum-group minerals in Alpine chromitites from southwestern Oregon. *Econ. Geol.* **79**, 491-508.

STUMPFL, E.F. (1974): The genesis of platinum deposits: further thoughts. *Minerals Sci. Engineering* **6**, 120-141.

TARKIAN, M., ECONOMOU-ELIOPOULOS, M. & SAMBANIS, G. (1996): Platinum-group minerals in chromitites from the Pindos ophiolite complex, Greece. *Neues Jahrb. Mineral., Monatsh.*, 145-160.

_____ & STUMPFL, E.F. (1975): Platinum mineralogy of the Driekop mine, South Africa. *Mineral. Deposita* **10**, 71-85.

TOLSTYKH, N.D., KRIVENKO, A.P., LAVRENT´EV, Y.G., TOLSTYKH, O.N. & KOROLYUK, V.N. (2000): Oxides of the Pd–Sb–Bi system from the Chiney Massif (Aldan Shield, Russia). *Eur. J. Mineral.* **12**, 431-440.

WAGNER, P. (1929): *The Platinum Deposits and Mines of South Africa*. Oliver & Boyd, Edinburgh, U.K.

WEISER, T.W. (1990): The quantitative proof of the existence of PGE-oxides. *Sixth Int. Platinum Symp.* (*Perth*), 52 (abstr.).

_____ (2002): Platinum-group minerals (PGM) in placer deposits. *In* The Geology, Geochemistry, Mineralogy and Mineral Beneficiation of Platinum-Group Elements (L.J. Cabri, ed.). *Can. Inst. Mining, Metall. Petroleum, Spec. Vol.* **54**, 721-756.

ZACCARINI, F., GARUTI, G. & CAWTHORN, R.G. (2002): Platinum-group minerals in chromitite xenoliths from the Onverwacht and Tweefontein ultramafic pipes, eastern Bushveld Complex. *Can. Mineral.* **40**, 481-497.

Received July 16, 2004, revised manuscript accepted May 31, 2005.